Cell Reports

Article

Muscle satellite cells are impaired in type 2 diabetic mice by elevated extracellular adenosine

Graphical abstract

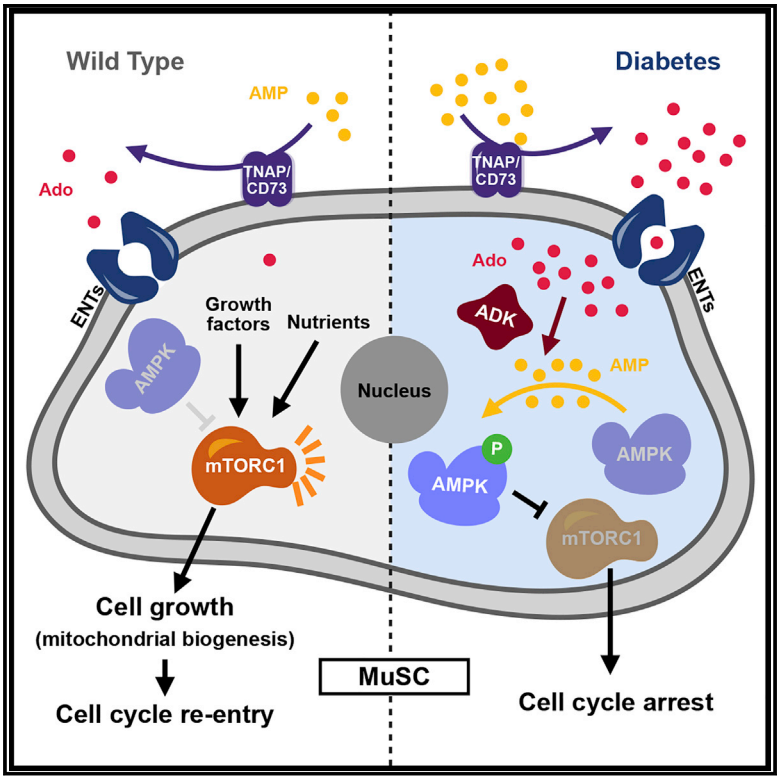

Highlights

- Elevated eAdo in diabetic mice impairs the regenerative functions of MuSCs
- eAdo inhibits mTORC1-dependent cell growth via the ENTs-ADK-AMPK axis
- Inhibition of either ENTs or ADK restores MuSC functions impaired by eAdo
- eAdo inhibits early activation of quiescent human MuSCs by the same mechanism

Authors

Lifang Han, Gang Wang, Shaopu Zhou, ..., Huating Wang, Jianfa Zhang, Zhenguo Wu

Correspondence

bczgwu@ust.hk

In brief

Han et al. reveal that elevated extracellular adenosine (eAdo) in diabetic mice impairs the regenerative functions of adult muscle stem cells (MuSCs) by inhibiting mTORC1 via the ENTs-ADK-AMPK signaling axis. Inhibition of ENTs or ADK restores MuSC functions compromised by eAdo, making them potential therapeutic targets in patients with diabetes.

Han et al., 2022, Cell Reports *39*, 110884
May 31, 2022
https://doi.org/10.1016/j.celrep.2022.110884

CellPress

Cell Reports

CellPress
OPEN ACCESS

Article

Muscle satellite cells are impaired in type 2 diabetic mice by elevated extracellular adenosine

Lifang Han,[1] Gang Wang,[1,9] Shaopu Zhou,[1] Chenghao Situ,[1] Zhiming He,[3] Yuying Li,[4] Yudan Qiu,[1] Yu Huang,[5] Aimin Xu,[6] Michael Tim Yun Ong,[7] Huating Wang,[4] Jianfa Zhang,[8] and Zhenguo Wu[1,2,10,*]

[1]Division of Life Science, the State Key Laboratory on Molecular Neuroscience, the Hong Kong University of Science & Technology, Hong Kong, China
[2]Greater Bay Biomedical Innocenter, Shenzhen Bay Laboratory, Shenzhen, 518055, China
[3]Department of Chemical Pathology, the Chinese University of Hong Kong, Hong Kong, China
[4]Li Ka Shing Institute of Health Sciences, Department of Orthopaedics and Traumatology, the Chinese University of Hong Kong, Hong Kong, China
[5]Department of Biomedical Sciences, the City University of Hong Kong, Hong Kong, China
[6]Department of Medicine, the University of Hong Kong, Hong Kong, China
[7]Department of Orthopaedics and Traumatology, the Chinese University of Hong Kong, the Prince of Wales Hospital, Hong Kong, China
[8]Nanjing University of Science and Technology, Nanjing, 210094, China
[9]Present address: Department of Immunology, Harvard Medical School. Boston, MA 02115, USA
[10]Lead contact
*Correspondence: bczgwu@ust.hk
https://doi.org/10.1016/j.celrep.2022.110884

SUMMARY

Muscle regeneration is known to be defective under diabetic conditions. However, the underlying mechanisms remain less clear. Adult quiescent muscle satellite cells (MuSCs) from leptin-receptor-deficient (i.e., *db/db*) diabetic mice are defective in early activation *in vivo*, but not in culture, suggesting the involvement of pathogenic niche factors. Elevated extracellular adenosine (eAdo) and AMP (eAMP) are detected under diabetic conditions. eAdo and eAMP potently inhibit cell cycle re-entry of quiescent MuSCs and injury-induced muscle regeneration. Mechanistically, eAdo and eAMP engage the equilibrative Ado transporters (ENTs)-Ado kinase (ADK)-AMPK signaling axis in MuSCs to inhibit the mTORC1-dependent cell growth checkpoint. eAdo and eAMP also inhibit early activation of quiescent fibroadipogenic progenitors and human MuSCs by the same mechanism. Treatment of *db/db* diabetic mice with an ADK inhibitor partially rescues the activation defects of MuSCs *in vivo*. Thus, both ADK and ENTs represent potential therapeutic targets for restoring the regenerative functions of tissue stem cells in patients with diabetes.

INTRODUCTION

Diabetes mellitus (DM) is a chronic metabolic disease that is usually accompanied with other complications, such as cardiovascular dysfunction, vision loss, and kidney failure (Cole and Florez, 2020; Ritchie and Abel, 2020; Zheng et al., 2018). Among various reported mechanisms underlying the pathogenesis of diabetes, purinergic signaling has also been linked to the development of the disease (Antonioli et al., 2015; Pardo et al., 2017; Peleli and Carlstrom, 2017). This pathway is initiated by extracellular ATP (eATP) that is released by various cell types in response to inflammation, hypoxia, or tissue injury (Dosch et al., 2018; Faas et al., 2017). eATP acts on target cells via two types of P2 receptors: the P2X receptors (P2XRs) and the P2Y receptors (P2YRs) (Cekic and Linden, 2016; Faas et al., 2017). eATP elicits strong proinflammatory responses (Rossi et al., 2012). In addition, eATP can also be quickly hydrolyzed to ADP and AMP by plasma membrane-bound ectonucleotidases (like CD39), and AMP can be further hydrolyzed to adenosine (Ado) by other membrane-bound ectonucleotidases (like CD73) (Allard et al., 2020; Boison and Yegutkin, 2019). Unlike eATP, extracellular Ado (eAdo) mainly elicits immunosuppressive responses via four G protein-coupled receptors (also called P1 purinergic receptors): A1, A2a, A2b, and A3 (Allard et al., 2020; Antonioli et al., 2013; Cronstein and Sitkovsky, 2017). Moreover, eAdo can also be transported back to the cytoplasm of target cells by the SLC28 family of concentrative nucleoside transporters (CNTs) or the SLC29 family of equilibrative nucleoside transporters (ENTs) (Boison and Yegutkin, 2019; Pastor-Anglada and Pérez-Torras, 2018). Once inside cells, Ado can be either phosphorylated to AMP by adenosine kinase (ADK) or deaminated to inosine by adenosine deaminase (ADA) (Boison and Yegutkin, 2019). The levels of eATP, eAMP, and eAdo were found to be elevated in both patients with diabetes and diabetic rodents (Dudzinska, 2014; Varadaiah et al., 2019; Xiang et al., 2018; Yang et al., 2019a; Zhang et al., 2012). Purinergic signaling has also been

shown to regulate glucose homeostasis, β cell proliferation, and insulin sensitivity (Antonioli et al., 2015; Johansson et al., 2007; Pardo et al., 2017).

Skeletal muscle, the major tissue for glucose and fatty acid utilization (Ceddia, 2005; Corcoran et al., 2007), exhibits impaired regenerative abilities in various diabetic animal models (Arounleut et al., 2013; D'Souza et al., 2016; Fu et al., 2016; Nguyen et al., 2011). However, the underlying mechanisms remain poorly understood. Muscle satellite cells (MuSCs) are responsible for injury-induced muscle regeneration. MuSCs uniquely express Pax7 and are sandwiched between the plasma membrane of individual myofibers and the surrounding basal lamina (Evano and Tajbakhsh, 2018; van Velthoven and Rando, 2019; Yin et al., 2013; Relaix et al., 2021). In uninjured adult muscles, MuSCs are quiescent with small cell size, low RNA content, and low metabolic activities (Evano and Tajbakhsh, 2018; Relaix et al., 2021; van Velthoven and Rando, 2019). Upon muscle injury, quiescent MuSCs (QSCs) are quickly activated to become activated satellite cells (ASCs), a process involving quick activation of the phosphatidylinositol 3-kinase (PI3K) pathway, rapid induction of immediate-early genes (e.g., *Jun*, *Fos*, *Egr*, and *Myc*), and expression of MyoD protein (Machado et al., 2017, 2021; van Velthoven et al., 2017; Wang et al., 2018). ASCs further undergo a period of cell growth, which is manifested by an obvious increase in cell size, enhanced mitochondria biogenesis, and activation of multiple anabolic pathways, before they re-enter the cell cycle to become proliferating myoblasts (Rocheteau et al., 2012; Rodgers et al., 2014; Zhou et al., 2021). The latter can then undergo either terminal differentiation or self-renewal to complete the muscle regeneration process (Evano and Tajbakhsh, 2018; Yin et al., 2013). Upon activation, it takes ~36–48 h for QSCs to re-enter the first cell cycle. However, it only takes ~8–10 h for the cycling myoblasts to finish subsequent cell cycles (Rocheteau et al., 2012; Rodgers et al., 2014; Wang et al., 2018; Zhou et al., 2021). The prolonged period required by QSCs to re-enter the first cell cycle ensures that appropriate changes occur at the epigenetic, transcriptional, translational, and metabolic levels before cells are ready for cell division. Any defect that interferes with such changes during this initial extended period could lead to impaired muscle regeneration. Indeed, we and others have found that the PI3K signaling pathway regulates a critical early activation checkpoint (García-Prat et al., 2020; Wang et al., 2018; Yue et al., 2017). Recently, we also identified another cell growth checkpoint during this early transition period that controls enhanced mitochondria biogenesis and activation of anabolic pathways (Zhou et al., 2021). In addition to intrinsic factors, niche is also known to regulate adult MuSCs (Baghdadi and Tajbakhsh, 2018; Fuchs and Blau, 2020; Relaix et al., 2021; Yin et al., 2013). For example, Fibronectin was shown to regulate both maintenance and expansion of MuSCs (Bentzinger et al., 2013; Lukjanenko et al., 2016). Moreover, by binding to calcitonin receptor on MuSCs, MuSC-secreted collagen V also contributes to Notch-induced quiescence maintenance (Baghdadi et al., 2018). While it is important to elucidate mechanisms that regulate stem cells under normal physiological conditions, it is also essential to understand how stem cells are affected under pathological conditions.

Here, we showed that eAdo (and eAMP) functions as a key pathogenic niche factor in diabetic mice to impair the regenerative functions of adult MuSCs. By specifically engaging the ENTs-ADK-AMPK signaling axis, eAdo inhibited the mTORC1-dependent cell growth checkpoint in QSCs and prevented them from re-entering the cell cycle, which ultimately impaired injury-induced muscle regeneration. Prolonged inhibition of ADK *in vivo* in diabetic mice partially rescued the cell cycle re-entry defect of their MuSCs.

RESULTS

Injury-induced muscle regeneration was impaired in type 2 diabetic mouse models

Several groups reported that the regenerative ability of skeletal muscle was impaired in obese or diabetic mice (Arounleut et al., 2013; D'Souza et al., 2016; Fu et al., 2016; Nguyen et al., 2011). However, the underlying mechanisms remained obscure. To further understand how adult MuSCs were affected under diabetic conditions, we started by confirming previous findings using two different type 2 diabetic mouse models: one (C57BL/6J) was created by high-fat diet (HFD) and a single dose of streptozotocin (STZ) injection, while the other was created by a recessive mutation in the leptin receptor gene (the *db*/*db* mice) (Kleinert et al., 2018). To assess the muscle regenerative functions *in vivo*, we induced acute muscle injury by injection of cardiotoxin (CTX) into the tibialis anterior (TA) muscle of diabetic *db*/*db* mice and examined the TA muscle at different days postinjury (dpi). In *db*/+ non-diabetic control mice, by 4.5 dpi, multiple small regenerating myofibers had already appeared on muscle sections. However, few were found on the muscle sections from *db*/*db* mice (Figure S1A, top panel). Consistently, by immunostaining for embryonic myosin heavy chain (eMHC), a protein that was transiently expressed in early-regenerating myofibers (d'Albis et al., 1988), we detected smaller $eMHC^+$ myofibers on muscle sections from *db*/*db* mice (Figures S1B and S1C). However, by 14 or 30 dpi, the injured muscles were fully repaired in *db*/*db* mice, suggesting that MuSCs were defective but not totally non-functional in *db*/*db* mice (Figure S1A middle and bottom panels). Similarly, in the HFD-fed and STZ-induced diabetic mice, at 4.5 dpi, there were also fewer regenerating myofibers compared with the muscle sections from the age- and gender-matched lean mice (Figure S1D). Taken together, these results confirmed previous findings that the regenerative ability of skeletal muscle was indeed impaired in diabetic mice.

MuSCs from *db/db* mice were defective in cell cycle re-entry *in vivo* but not *in vitro*

To examine the functions of MuSCs in diabetic mice, we decided to focus on *db*/*db* mice in the following studies. We first enumerated MuSCs in uninjured hindlimb muscles from young (1-month-old) and adult (≥3-month-old) mice by fluorescence-activated cell sorting (FACS). The purity of the freshly isolated MuSCs (FISCs) was more than 90% as judged by immunostaining for Pax7 (Figure S2A). While the number of MuSCs in young *db*/*db* mice was slightly lower than that of the control mice (i.e., *db*/+), the difference was not significant (Figure S2B). However, the number of MuSCs decreased by ~50% in adult *db*/*db* mice

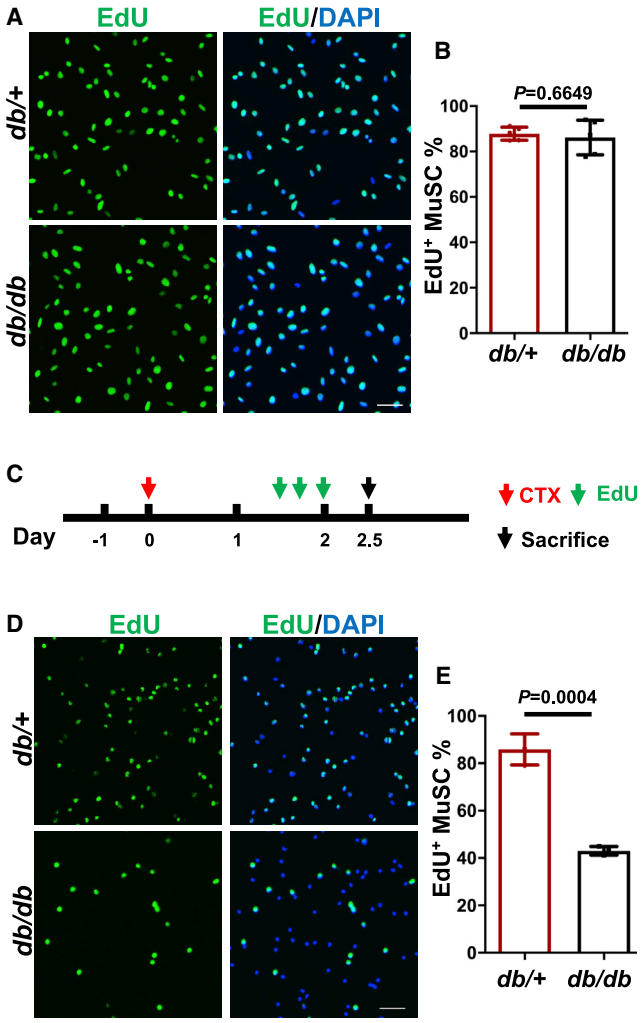

Figure 1. MuSCs from *db/db* mice showed cell cycle re-entry defect *in vivo* but not *in vitro*

(A) An equal number of FISCs from adult *db*/+ and *db/db* mice were cultured in the presence of EdU (10 μM) for 48 h. Cells were fixed and stained for EdU (green).

(B) Quantification of the percentage of EdU$^+$ MuSCs from (A) (n = 5 mice/group).

(C) Experimental scheme: adult *db*/+ and *db/db* mice were injured with CTX in the lower hindlimb muscle. At 1.5 dpi, EdU was i.p. injected into the mice every 6 h for three doses. Mice were sacrificed at 2.5 dpi and an equal number of FISCs from injured lower hindlimb muscles were immediately subjected to EdU staining.

(D) Representative images from the *in vivo* EdU incorporation assays.

(E) Quantification of the percentage of EdU$^+$ MuSCs from (D) (n = 3 mice/group). In (A) and (D), nuclei were counterstained with DAPI (blue). In (B) and (E), data were presented as mean ± SD. Scale bars: 50 μm. See also Figures S1, S2, and S3.

compared with littermate controls (Figure S2B). Consistently, by immunostaining for Pax7, we also detected significantly fewer MuSCs on muscle sections (Figures S2C and S2D) from adult but not young *db/db* mice. Next, we examined whether MuSCs from adult *db/db* mice could undergo proper activation, proliferation, and differentiation. To examine how MuSCs behave in early activation, we isolated MuSCs from *db*/+ and *db/db* mice by FACS and cultured the same number of FISCs for 48 h in the presence of 5-ethynyl-2′-deoxyuridine (EdU) (Zhou et al., 2021). By this time, a similar percentage (~85%) of FISCs from either *db*/+ or *db/db* mice became EdU$^+$ (i.e., re-entered the first cell cycle) (Figures 1A and 1B). Consistently, using isolated single myofibers that were cultured in suspension together with EdU for 48 h, nearly all MuSCs that remained attached to myofibers became EdU$^+$ no matter whether they were isolated from *db*/+ or *db/db* mice (Figures S2E and S2F). By culturing FISCs or single myofibers for 72 h, we found that FISCs or SCs attached to single myofibers from *db/db* mice were comparable with their counterparts from *db*/+ mice in proliferation and differentiation in culture (Figures S2G–S2J). Our assays above revealed that MuSCs from *db/db* mice were comparable with their counterparts from *db*/+ mice in early activation, proliferation, and differentiation in culture. Next, we examined early activation of MuSCs *in vivo*. Following the scheme in Figure 1C, we found that ~85% of MuSCs from the *db*/+ mice already incorporated EdU, whereas only ~40% of MuSCs from *db/db* mice did so (Figures 1D and 1E), indicative of an obvious cell cycle re-entry defect in MuSCs from *db/db* mice *in vivo*. The differential behaviors of MuSCs from *db/db* mice in culture and *in vivo* during early activation suggested the involvement of certain pathogenic niche factors *in vivo*. Next, we also assessed the self-renewal ability of MuSCs in *db/db* mice *in vivo*. One month after CTX-induced muscle injury, the number of self-renewed MuSCs was about two to three times that in uninjured muscles from *db*/+ control mice as judged by either FACS analysis or immunostaining of muscle sections (Figure S3), which was often observed in wild-type adult mice (Li et al., 2019). In contrast, such an increase in the number of self-renewed MuSCs was barely detected in *db/db* mice (Figure S3), suggesting that MuSCs in *db/db* diabetic mice were partially defective in self-renewal, which could also be caused by pathogenic niche factors.

Elevated eAdo and eAMP impaired the functions of MuSCs both in culture and *in vivo*

We and others previously reported that the levels of eAMP and eAdo were elevated in both diabetic mice and patients with diabetes (Dudzinska, 2014; Varadaiah et al., 2019; Xiang et al., 2018; Yang et al., 2019a; Zhang et al., 2012). As both eAMP and eAdo were known to exert deleterious effects on various tissues/cells (Idzko et al., 2014; Zhang et al., 2011), we hypothesized that elevated levels of eAdo or eAMP impair MuSC functions in diabetic mice. To test this hypothesis, we first monitored cell cycle re-entry of FISCs from adult wild-type mice in culture upon eAMP or eAdo treatment and found that both potently inhibited cell cycle re-entry of FISCs in a dose-dependent manner (Figures 2A–2D). We further examined the impact of elevated eAMP on MuSC functions *in vivo* by performing $BaCl_2$-induced injury-regeneration assays with daily intraperitoneal (i.p.) injection of AMP or vehicle (Figure 2E, top). By 4.5 dpi, multiple small regenerating myofibers already appeared on muscle sections from vehicle-treated mice as expected (Figure 2E, left panels). However, few such myofibers were found on muscle sections from AMP-treated mice (Figure 2E, right panels), indicating that

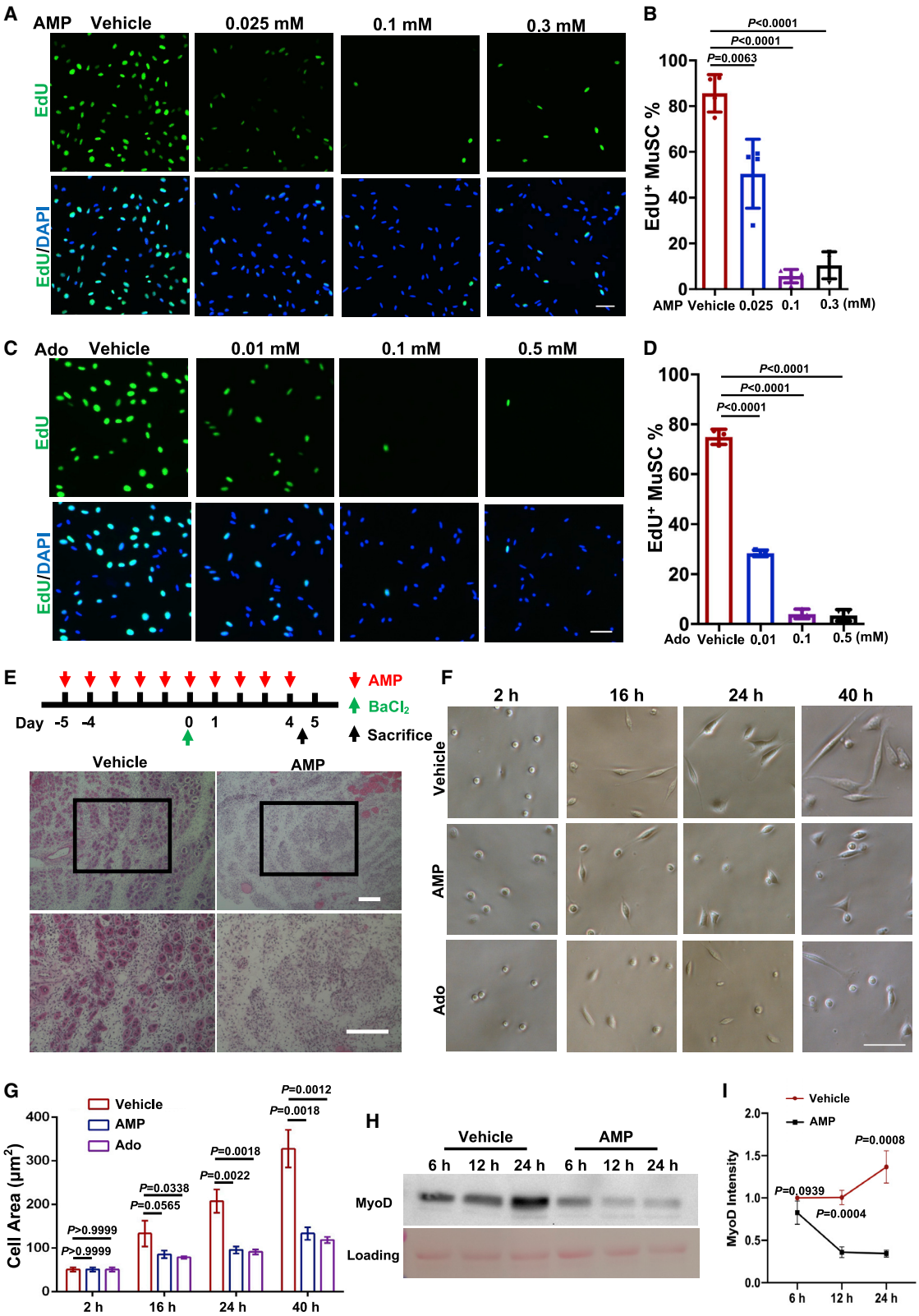

(legend on next page)

elevated levels of eAMP indeed impaired the functions of MuSCs *in vivo*. We next tried to determine when AMP- or Ado-triggered defects occurred in MuSCs during their early activation. We first monitored the gradual change in cell size upon activation of MuSCs in culture with or without eAMP or eAdo (Evano and Tajbakhsh, 2018; van Velthoven and Rando, 2019; Zhou et al., 2021). As expected, the size of FISCs treated by vehicle (i.e., DMSO) obviously increased after cells were grown in culture for 16–24 h, and peaked by ~40 h in culture (Figures 2F and 2G). For FISCs treated by eAMP or eAdo, their sizes also slightly increased during the initial 16–24 h of growth in culture (Figures 2F and 2G). However, the extent of the increase in eAMP- or eAdo-treated MuSCs was much less than that in vehicle-treated controls. Moreover, a further increase in cell size between 24 and 40 h was more severely impaired in eAMP- or eAdo-treated MuSCs (Figures 2F and 2G). As MyoD protein expression is another early marker of ASCs (Yin et al., 2013; Zhou et al., 2021), we also examined it by western blot. After 6 h in culture, the protein levels of MyoD were comparable between ASCs treated with vehicle and eAMP (Figures 2H and 2I). A further induction of MyoD protein occurred in vehicle-treated ASCs after they were grown in culture for 24 h. However, this further induction of MyoD protein was totally inhibited by eAMP (Figures 2H and 2I). Our data above suggested that eAMP and eAdo had little or no effect on the early-activation checkpoint regulated by PI3K (Wang et al., 2018). Instead, they mainly impaired the subsequent cell growth checkpoint (Zhou et al., 2021).

eAdo/eAMP inhibited mTORC1 and mitochondria biogenesis

To further understand why Ado or AMP treatment prevented MuSCs from re-entering the cell cycle upon activation, we set out to examine the transcriptomes of ASCs with or without eAdo/eAMP treatment by RNA sequencing (RNA-seq). As the activation defect caused by eAMP or eAdo appeared to occur at the cell growth checkpoint (Figures 2F–2I), we decided to examine the transcriptomes of ASCs after treatment of FISCs with eAdo or eAMP in culture for 24 h (Zhou et al., 2021). Principal component analysis (PCA) revealed good reproducibility among biological triplicates in each group and clear separation between vehicle-treated and Ado- or AMP-treated ASCs (Figure S4A). Moreover, in the PCA plot, ASCs treated by eAdo and eAMP were clustered together, suggesting that they elicited very similar transcriptomic changes, which was also confirmed by scatterplot analysis and Venn diagram (Figures S4B and S4C). A heatmap displaying the top 50 differentially expressed genes (DEGs) in Ado- or AMP-treated ASCs also confirmed such findings (Figure S4D). We then performed gene set enrichment analysis (GSEA) to identify dysregulated pathways or biological processes in both Ado- and AMP-treated ASCs (Subramanian et al., 2005). Notably, many cell-cycle-related terms, like "E2F targets," "G2M checkpoint," "Myc targets," and "mitotic spindle," were all enriched in control ASCs (Figure 3A). Consistently, genes involved in G1/S transition (e.g., *E2f1-3*, *Ccne1/2*, *Cdk2*, and *Cdk6*) (Figure S4E) and DNA replication origin licensing (e.g., *Cdc6*, *Cdt1*, and *Mcm2-7*) (Figure S4F) were all poorly expressed in Ado- and AMP-treated ASCs. By contrast, genes related to inflammatory responses and stress-related pathways, including p53 pathway, interferon α and γ responses, TNFα signaling via NF-κB, IL-6 JAK STAT3 signaling, hypoxia, and apoptosis, were enriched in Ado- and AMP-treated ASCs (Figure 3A). These GSEA features were very similar to that seen in Paxbp1-null ASCs (Zhou et al., 2021), further supporting our hypothesis that the cell growth checkpoint was impaired in Ado- and AMP-treated ASCs. To ascertain whether this is the case, we first turned to mitochondria as ASCs with a defective cell growth checkpoint are known to have impaired mitochondria biogenesis and defective respiratory functions (Zhou et al., 2021). We monitored mitochondria biogenesis by staining for Tomm20, a known mitochondria-resident protein, in ASCs with or without AMP or Ado treatment. While few mitochondria were detected in FISCs cultured for 2 h, mitochondrial biogenesis became obvious in control ASCs after 16–24 h in culture, as shown by an enhanced Tomm20 signal, which further increased by 36 h (Figures 3B and 3C). In ASCs treated with AMP or Ado, mitochondrial biogenesis was obviously suppressed based on the decreased Tomm20 signal (Figures 3B and 3C). As peroxisome proliferator-activated receptor-gamma coactivator 1 (PGC1) is a master regulator for mitochondrial biogenesis, we also examined its mRNA and protein expression. Based on our RNA-seq data, *Ppargc1b* (encoding PGC1β) was downregulated by ~5- and 10-fold in AMP- and Ado-treated ASCs, respectively (Figure 3D). Consistently, by western blot, we also confirmed its decreased protein levels in AMP- and Ado-treated ASCs (Figure 3E). To assess the respiratory functions of mitochondria in ASCs, we grew FISCs in culture for various times with or without Ado or AMP treatment

Figure 2. eAdo and eAMP impaired the cell growth checkpoint during early activation of MuSCs

(A–D) FISCs were cultured with EdU with or without eAMP (A and B) or eAdo (C and D) for 48 h, followed by cell fixation and staining for EdU (green) and DAPI (blue).

(B and D) Quantification of the percentage of EdU^+ MuSCs in (A) and (C), respectively (n = 4 for A; and n = 3 for C).

(E) Top: experimental scheme: 2-month-old mice were i.p. injected with five consecutive doses of AMP (10 mg/mouse), and then injured with $BaCl_2$ in TA muscles, followed by another five consecutive doses of AMP after injury. Mice were sacrificed at 4.5 dpi and TA muscle sections were subjected to H&E staining. Bottom: representative images (n = 3 mice/group).

(F) FISCs were cultured with or without eAMP or eAdo and representative bright-field images were taken at various times as indicated.

(G) Quantification of mean cell sizes in (F) by Fiji (ImageJ): at each time point, >100 cells from three independent experiments were measured.

(H) FISCs were cultured with or without eAMP (0.25 mM) and harvested at various time points. Whole-cell lysates (WCLs) were subjected to western blotting.

(I) Quantification of data in (H) by densitometry (n = 3).

Data are presented as mean ± SD.

Scale bars: 50 μm in (A), (C), and (F), and 100 μm in (E).

A

Enriched in DMSO	Enriched in Ado & AMP
E2F TARGETS	INTERFERON ALPHA RESPONSE
G2M CHECKPOINT	TNFA SIGNALING VIA NFKB
MYC TARGETS V1	P53 PATHWAY
MTORC1 SIGNALING	INTERFERON GAMMA RESPONSE
MITOTIC SPINDLE	IL6 JAK STAT3 SIGNALING
MYC TARGETS V2	APOPTOSIS
APICAL JUNCTION	XENOBIOTIC METABOLISM
WNT BETA CATENIN SIGNALING	INFLAMMATORY RESPONSE
GLYCOLYSIS	HYPOXIA
ESTROGEN RESPONSE LATE	
APICAL SURFACE	

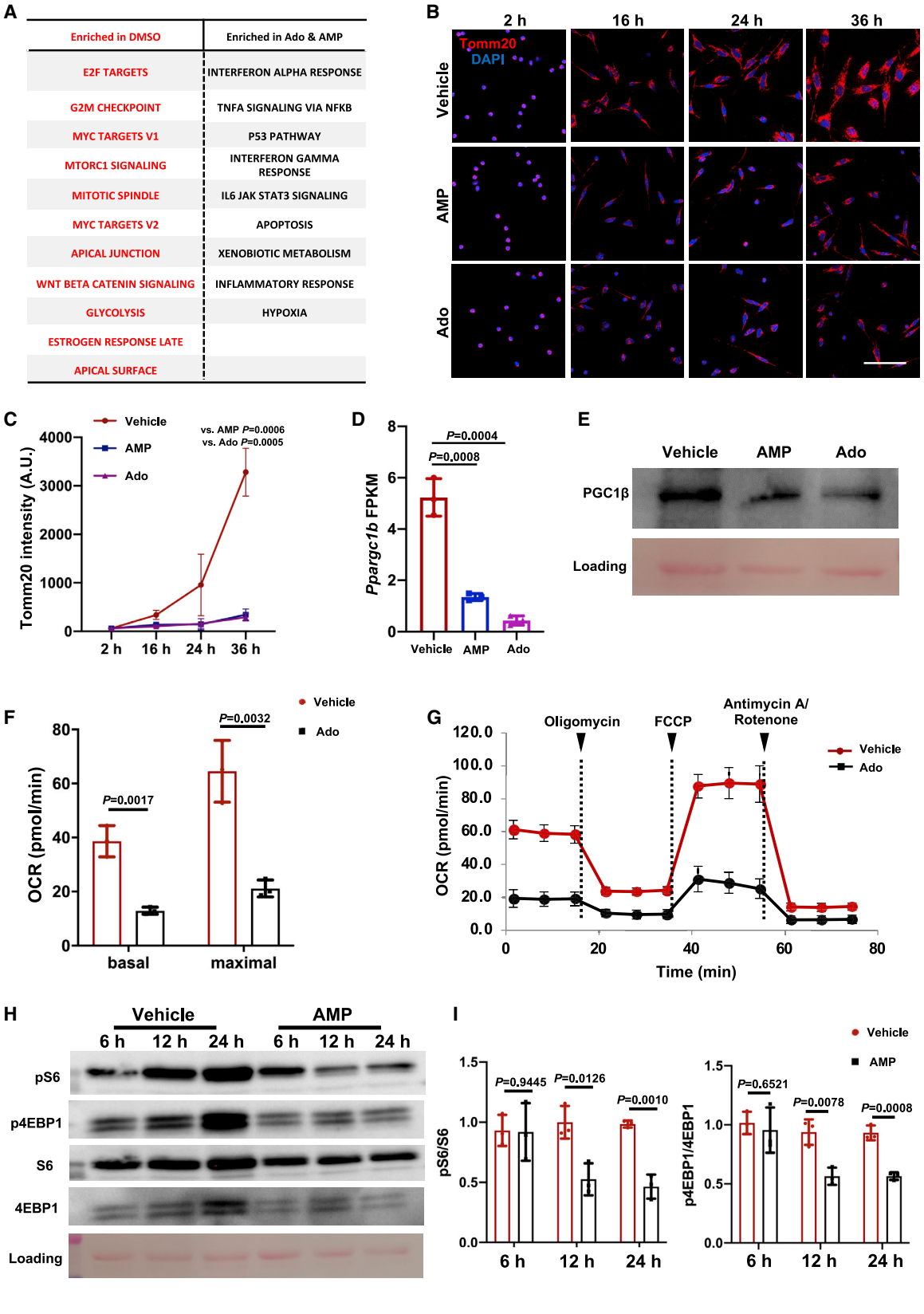

(legend on next page)

and then assessed the activity of the electron transport chain (ETC) by measuring the oxygen consumption rate (OCR). We found that both Ado- and AMP-treated ASCs were severely defective in ETC-dependent cellular respiration as shown by reduced basal and maximal OCR (Figures 3F, 3G, and S5A). Our recent work revealed that an elevated mTORC1 activity is the main driving force for enhanced mitochondrial biogenesis and respiratory functions and critically regulates the cell growth checkpoint (Zhou et al., 2021). If Ado or AMP indeed impaired the cell growth checkpoint, it was likely that they did so by targeting mTORC1. Indeed, our GSEA revealed that genes related to mTORC1 signaling were downregulated in ASCs treated with either Ado or AMP (Figure 3A). Consistently, by examining the phosphorylated ribosomal protein S6 (pS6) and 4EBP1 (p4EBP1), two widely used readouts of the mTORC1 activity (Liu and Sabatini, 2020), we found that the elevated mTORC1 activity in ASCs that had been cultured for 12–24 h was obviously suppressed by AMP or Ado treatment (Figures 3H, 3I, and S5B–S5D). Next, we tested whether hyperactivation of mTORC1 could rescue the activation defects in Ado- or AMP-treated ASCs. To do so, we induced MuSC-specific *Pten* deletion in adult *Pax7*$^{CreER/CreER}$; *Pten*$^{flox/-flox}$; *R26*$^{YFP/YFP}$ mice. As expected, loss of Pten, a potent negative regulator of the PI3K/mTORC1 pathway (Liu and Sabatini, 2020), in FISCs led to an elevated mTORC1 activity, as shown by increased pS6 protein levels (Figure 4A). When we treated FISCs from heterozygous control and *Pten*-knockout (KO) mice with or without Ado or AMP, as expected, both Ado and AMP potently inhibited EdU incorporation in control ASCs. However, such an activation defect caused by Ado or AMP was partially rescued in *Pten*-null ASCs, as shown by much more EdU$^+$ *Pten*-null ASCs (Figures 4B and 4C). Taken together, our data above showed that eAdo/eAMP inhibited the mTORC1-dependent cell growth checkpoint.

eAdo/eAMP suppressed early activation of MuSCs through ENTs and ADK

We next examined how eAdo and eAMP exerted their effects on MuSCs. Ado could presumably exert its effect on target cells through either Ado receptors or Ado transporters (Allard et al., 2020; Boison and Yegutkin, 2019). To determine which of them actually mediated the inhibitory effect of Ado on early activation of MuSCs, we treated FISCs from wild-type mice with Ado in the absence or presence of dipyridamole and CGS15943, the pan-inhibitors for ENTs and Ado receptors, respectively (Holtzman, 1996; Yao et al., 1997). As expected, eAdo treatment potently suppressed cell cycle re-entry of FISCs, as shown by the presence of few EdU$^+$ cells. Interestingly, dipyridamole dose-dependently restored the percentage of EdU$^+$ cells close to that in control SCs (Figures 5A and 5B). By contrast, CGS15943 had no such rescuing effect on eAdo-treated SCs (our unpublished data). As to eAMP, no membrane-bound AMP-specific transporters or receptors were known to exist. Neither was the negatively charged AMP expected to passively diffuse into target cells. As genes encoding several ectonucleotidases (like *Alpl* and *Nt5e*, which encode tissue non-specific alkaline phosphatase or TNAP and CD73, respectively) were expressed in FISCs (Wang et al., 2018; Zhou et al., 2021), it was likely that eAMP was first hydrolyzed to Ado by TNAP or CD73, which in turn exerted its effects through ENTs. This hypothesis was supported by similar transcriptomic changes in ASCs elicited by AMP or Ado (Figure S4). To further test this hypothesis, we treated FISCs with eAMP in the absence or presence of dipyridamole or CGS15943. Indeed, eAMP-mediated suppression of EdU incorporation in ASCs was effectively rescued by dipyridamole in a dose-dependent manner (Figures S6A and S6B). CGS15943 had no such rescuing effects (our unpublished data). After entering cells, Ado could be metabolized to either inosine by ADA or AMP by ADK. AMP in turn could be further converted to either IMP by AMP deaminase or ADP by adenylate kinase (AK). To investigate which of these enzymes was involved in mediating the inhibitory effect of eAdo on MuSCs, we treated FISCs with eAdo in the absence or presence of various inhibitors for these enzymes and then monitored EdU incorporation in culture. Although the inhibitors for ADA, AMP deaminase, or AK had no obvious effect in restoring decreased EdU incorporation in Ado-treated SCs (our unpublished data), ABT-702, a specific ADK inhibitor (ADKI) (Jarvis et al., 2000), largely rescued the cell cycle re-entry defect caused by Ado (Figures 5C and 5D). Similarly, reduced EdU incorporation in eAMP-treated ASCs was also efficiently rescued by ABT-702 but not by other inhibitors (Figures S6C and S6D). Moreover, 5-iodotubercidin, another specific ADKI structurally different from ABT-702, was as effective as ABT-702 in rescuing the cell cycle re-entry defect of MuSCs treated by either eAdo or eAMP (Figures S6E–S6H), which further strengthened our findings that ADK specifically mediates the effect of eAdo/eAMP on MuSCs. To further explore whether ADKI treatment could similarly rescue the early-activation defect of MuSCs *in vivo*, we chose diabetic *db/db* mice as our model as we previously showed that their MuSCs were

Figure 3. eAdo and eAMP impaired mitochondria biogenesis and respiratory functions in MuSCs by inhibiting mTORC1

(A) Enriched terms (false discovery rate [FDR] < 0.05) by GSEA based on RNA-seq are shown.

(B) FISCs were cultured with or without eAMP (0.25 mM) or eAdo (0.1 mM) for various times. Cells were fixed and stained for Tomm20 (red) and DAPI (blue). Representative fluorescent images are shown. Scale bar: 50 μm.

(C) Quantification of fluorescence intensity in (B) by Fiji (ImageJ): at each time point, >100 cells from three independent experiments were measured.

(D) The fragments per kilobase of transcript per million mapped reads (FPKM) values of *Ppargc1b* were shown (n = 3 mice/group).

(E) Representative western blot (n = 3) showing the protein levels of PGC1β in ASCs with or without eAMP or eAdo after 24 h in culture.

(F) Oxygen consumption rate (OCR) in ASCs treated with or without eAdo for 24 h (n = 3 mice/group). The changes in mean basal and maximal OCR are shown.

(G) Representative OCR plots for ASCs after 24 h in culture. FCCP, carbonyl cyanide 4-(trifluoromethoxy)phenylhydrazone.

(H) FISCs were cultured with or without eAMP for indicated times followed by western blotting.

(I) The band intensity in (H) was quantified by densitometry (n = 3).

Data are presented as mean ± SD.

See also Figures S4 and S5.

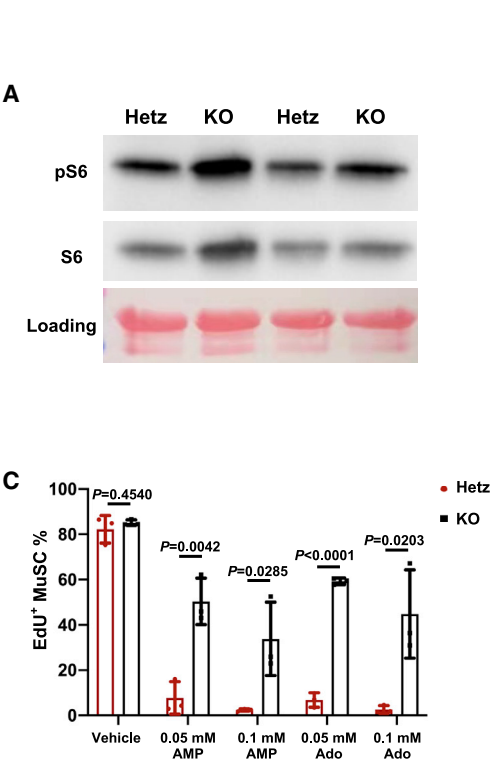

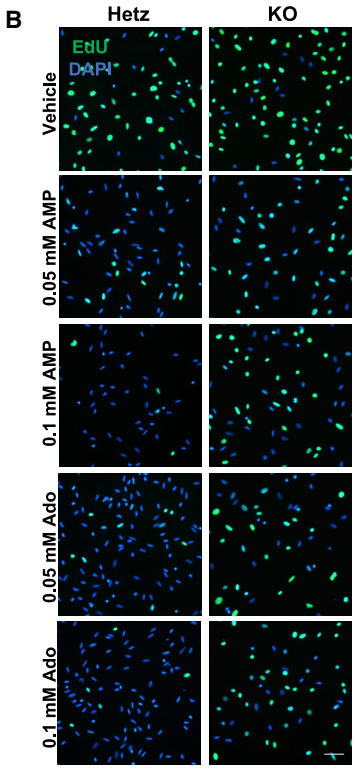

Figure 4. Hyperactivation of mTORC1 through *Pten* deletion partially rescued the cell cycle re-entry defect caused by eAdo or eAMP

(A) WCLs from the same number of FISCs from *Pten*-KO or heterozygous control (Hetz) mice were subjected to western blotting (n = 2).

(B) FISCs from *Pten*-KO or Hetz mice were cultured with EdU and different doses of eAMP or eAdo for 48 h followed by cell fixation and staining with EdU (green) and DAPI (blue). Representative fluorescent images are shown. Scale bar: 50 μm.

(C) Quantification of the percentage of EdU^+ MuSCs from (B) (n = 3). Data are presented as mean ± SD.

defective in cell cycle re-entry upon CTX-induced muscle injury (Figures 1C–1E). Following the scheme in Figure 5E, we showed that ABT-702 treatment had no obvious effect on EdU incorporation in ASCs from *db*/+ control mice, yet it partially rescued defective EdU incorporation in ASCs from *db*/*db* mice (Figures 5F and 5G). Collectively, our data above demonstrated that ENTs and ADK critically mediate the inhibitory effect of eAdo/eAMP on MuSCs.

eAdo/eAMP inhibited mTORC1 via AMPK

We showed that eAdo/eAMP impaired the early activation of MuSCs by inhibiting mTORC1 (Figures 3H, 3I, and S5B–S5D). It remained unclear how eAdo/eAMP did so. An obvious target is Paxbp1 as our recent work showed that it also regulates the cell growth checkpoint by inhibiting mTORC1 (Zhou et al., 2021). However, our RNA-seq data indicated that the mRNA levels of *Paxbp1* were not altered by Ado or AMP. As ADKI treatment rescued defective EdU incorporation in MuSCs treated by AMP or Ado, it was likely that ADKI did so by restoring the mTORC1 activity. To test this hypothesis, we treated FISCs with Ado or AMP for 24 h in culture in the absence or presence of ABT-702. We then determined the mTORC1 activity by western blot. While Ado or AMP treatment alone potently suppressed mTORC1 activity as we showed before, addition of ABT-702 together with Ado or AMP restored its activity close to the levels seen in the vehicle-treated control SCs (Figures 6A and 6B). The involvement of ADK (as well as ENTs) suggested that elevated levels of eAMP or eAdo could ultimately lead to elevated levels of intracellular AMP, which could in turn result in a higher intracellular [AMP]/[ATP] ratio and consequential activation of AMPK, a known suppressor of mTORC1 (Liu and Sabatini, 2020). To test this hypothesis, we treated FISCs with 0.25 mM AMP for various times and then measured the cellular AMP and ATP levels. Indeed, we found that eAMP induced a quick rise in the [AMP]/[ATP] ratio (Figure 6C). Consistently, using C2C12 myoblasts, we showed that AMP or Ado treatment induced AMPK activity as shown by elevated levels of p-Thr172-AMPK (Figures 6D and 6E), an active form of AMPK (Garcia and Shaw, 2017). Moreover, 5-aminoimidazole-4-carboxamide-1-β-4-ribo-furanoside (AICAR), a known agonist of AMPK (Towler and Hardie, 2007), inhibited both mTORC1 activity and EdU incorporation in FISCs in a dose-dependent manner (Figures 6F–6I). Taken together, we showed that eAdo/eAMP impaired mTORC1 activity via activation of AMPK.

eAdo/eAMP inhibited cell cycle re-entry of human MuSCs and fibroadipogenic progenitors by a conserved mechanism

To find out whether eAdo/eAMP also impaired early activation of adult human MuSCs, we isolated human MuSCs by FACS (Figure S7A) (Charville et al., 2015; Uezumi et al., 2016). The purity of human MuSCs was more than 90% as judged by immunostaining for either Pax7 in FISCs or MyoD in cultured SCs (Figures S7B–S7E). Similar to what we saw in mouse MuSCs, addition of AMP or Ado potently inhibited EdU incorporation in human MuSCs (Figures 7A and 7B). Importantly, addition of ABT-702 together with either AMP or Ado largely restored EdU incorporation close to the levels seen in vehicle-treated control SCs (Figures 7A and 7B). In diabetic *db*/*db* mice, both eAMP and eAdo were found to be elevated systemically (Dudzinska, 2014; Varadaiah et al., 2019; Xiang et al., 2018; Yang et al., 2019a; Zhang et al., 2012). As both ENTs and ADK are ubiquitously expressed, it is likely that eAdo/eAMP could also inhibit other quiescent cells during their early activation. To test this hypothesis, we turned to quiescent fibroadipogenic progenitors (FAPs) in uninjured skeletal muscle (Joe et al., 2010). Like

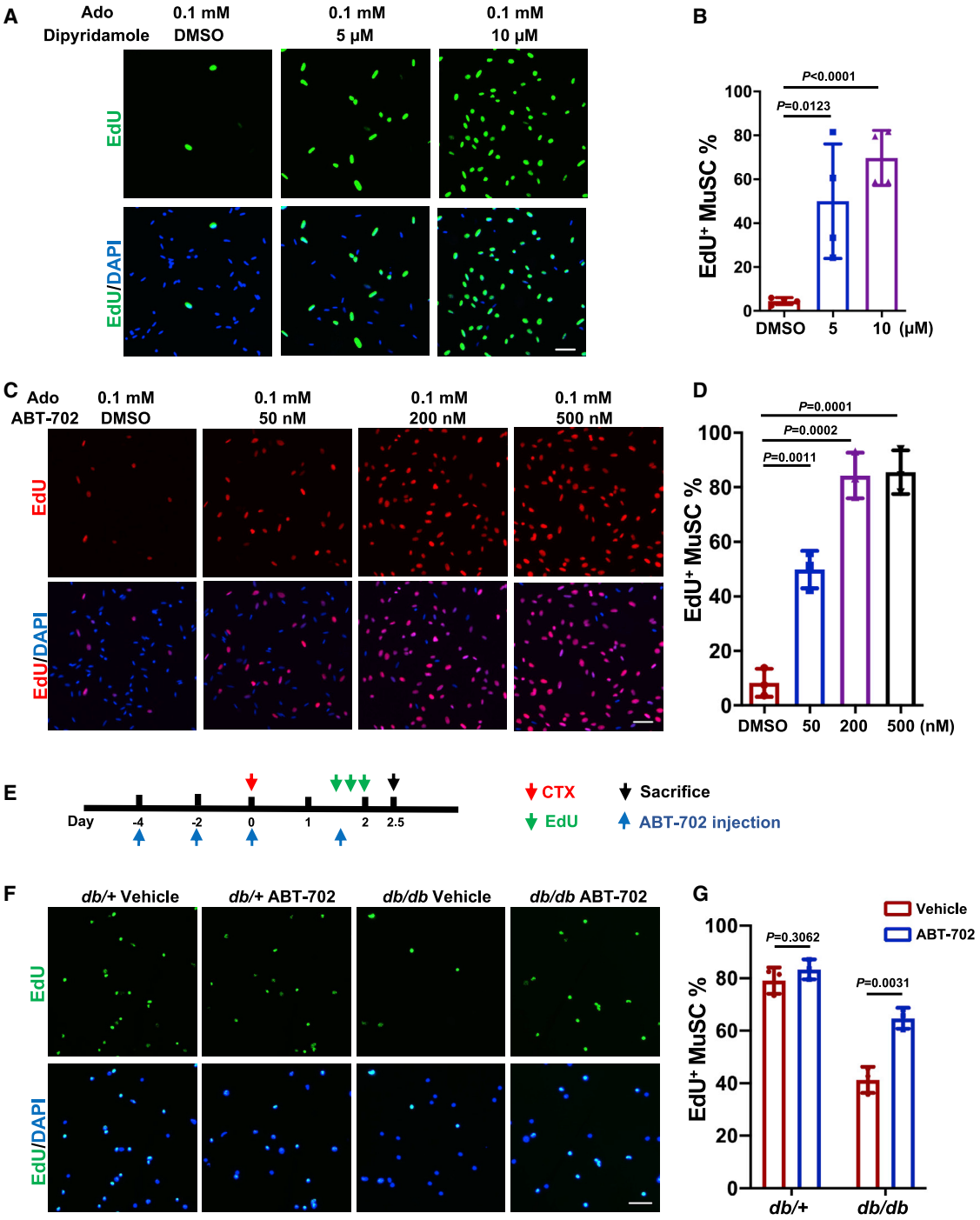

Figure 5. eAdo suppressed early activation of MuSCs through ENTs and ADK

(A–D) FISCs were cultured with EdU and eAdo with or without different does of dipyridamole (A, B) or ABT-702 (C, D) for 42 h followed by cell fixation and staining for EdU (green for A and red for C) and DAPI (blue).

(B and D) Quantification of the percentage of EdU$^+$ MuSCs in (A) and (C) (n = 4 for A and n = 3 for C).

(E) Experimental scheme: adult *db*/+ and *db*/*db* mice were i.p. injected with either ABT-702 (1.5 mg/kg mice) or 0.9% NaCl (vehicle) every other day for three doses, followed by CTX injury to the lower hindlimb muscles. At 1.5 dpi, EdU was i.p. injected into the mice together with another dose of ABT-702 followed by two more doses of EdU at 6 h apart. Mice were sacrificed at 2.5 dpi and FISCs from injured lower hindlimb muscles were subjected to EdU staining.

(F) Representative images of the *in vivo* EdU incorporation assays.

(G) Quantification of the percentage of EdU$^+$ MuSCs from (F) (n = 3 mice/group).

Data are presented as mean ± SD. Scale bars: 50 μm.

See also Figure S6.

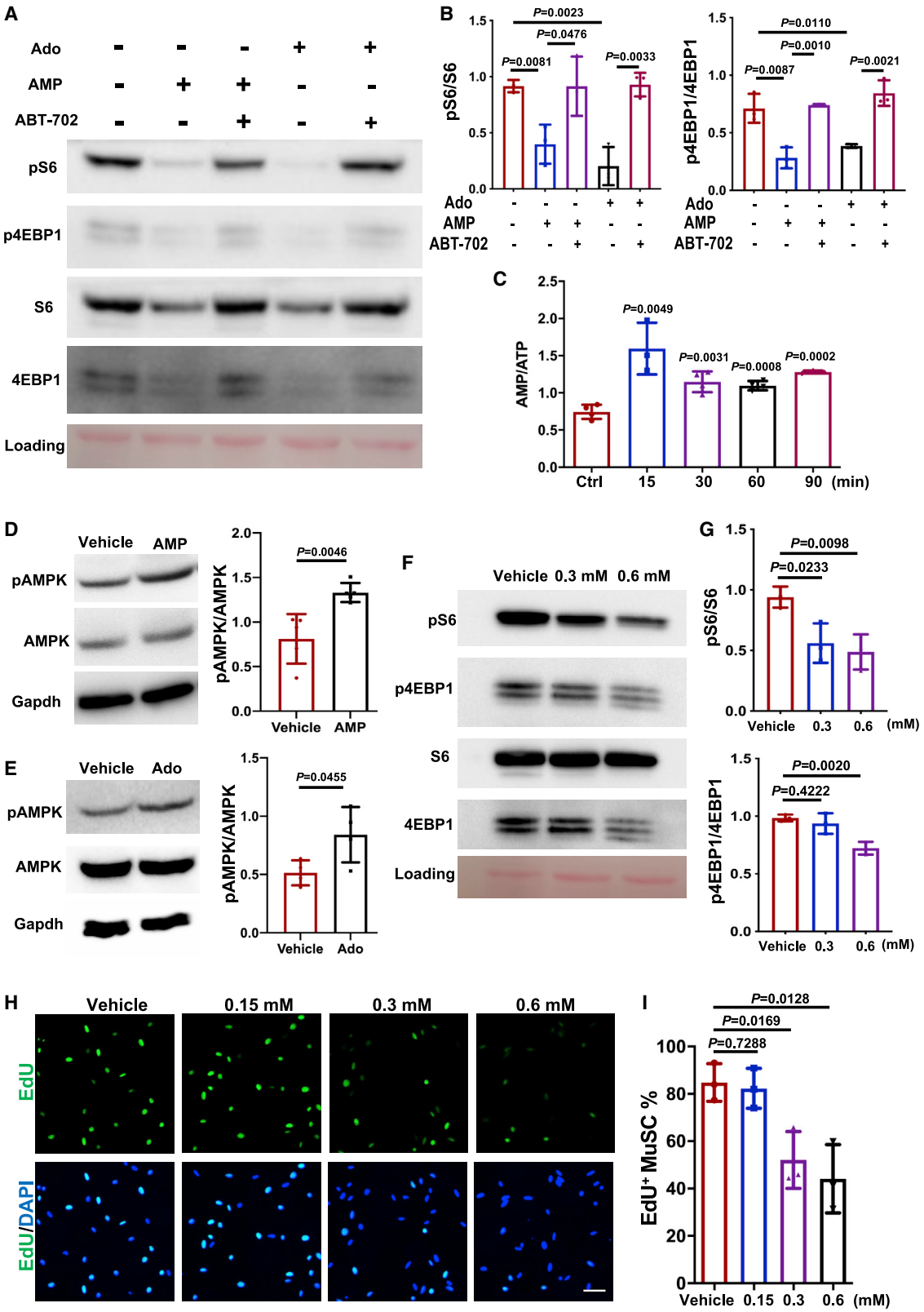

(legend on next page)

QSCs, FAPs were activated and re-entered the cell cycle to proliferate upon muscle injury *in vivo* or during growth in culture (Joe et al., 2010). We cultured freshly isolated FAPs in the presence of EdU for 48 h with or without AMP or Ado. Indeed, either eAdo or eAMP potently suppressed EdU incorporation in FAPs (Figures 7C and 7D). Importantly, ABT-702 effectively rescued the defects in EdU incorporation in FAPs treated by eAdo or eAMP (Figures 7C and 7D). Our data above indicated that eAdo/eAMP suppress activation of multiple quiescent cell types including FAPs and human MuSCs via the conserved ENTs-ADK signaling axis.

DISCUSSION

Purinergic signaling and diabetes

Purinergic signaling has been extensively studied in the past three decades (Burnstock, 2012, 2016). Most such studies focus on the opposing roles of eATP and eAdo during immune responses and tumor development (Allard et al., 2020; Cekic and Linden, 2016; Di Virgilio and Adinolfi, 2017). In normal healthy tissues, the levels of eATP and eAdo are very low (in the nanomolar range) (Di Virgilio et al., 2017; Faas et al., 2017). However, they can quickly rise to the micromolar range under pathological conditions like inflammation, hypoxia, and tissue damage (Cekic and Linden, 2016; Dosch et al., 2018; Faas et al., 2017). Dysregulated eATP-P2 receptor signaling has been linked to a number of human diseases (Di Virgilio and Adinolfi, 2017; Huang et al., 2021; Idzko et al., 2014). Similarly, disruption of Ado signaling also contributes to human diseases, including Parkinson's disease, cancer, and rheumatic diseases (Cronstein and Sitkovsky, 2017; Di Virgilio and Adinolfi, 2017; Stone et al., 2009). Purinergic signaling has also been studied in diabetes (Antonioli et al., 2015; Pardo et al., 2017; Peleli and Carlstrom, 2017). Ado was shown to regulate insulin secretion via A2a and β cell proliferation and survival (Antonioli et al., 2015). An agonist of A2b was found to have protective effects in type 1 diabetic mouse models by ameliorating destruction of β cells by the immune systems (Németh et al., 2007). Moreover, previous work from us and others showed that the levels of eAMP and eAdo were elevated in plasma or muscle of diabetic mice and in plasma of patients with diabetes (Dudzinska, 2014; Varadaiah et al., 2019; Xiang et al., 2018; Yang et al., 2019a; Zhang et al., 2012). We found that eAMP could regulate glucose homeostasis, insulin signaling, and the activity of hepatic protein tyrosine phosphatase 1B in *db/db* diabetic mice (Xia et al., 2015; Yang et al., 2019a, 2019b; Zhang et al., 2012). However, in either patients with diabetes or diabetic rodents, the exact cellular source of eAMP/eAdo remains unclear at present. Possible candidates include abundant adipocytes in obese *db/db* diabetic mice, red blood cells, and endothelial cells (Antonioli et al., 2015; Yang et al., 2019b).

eAdo suppresses early activation of quiescent adult stem and progenitor cells via a conserved ENTs-ADK signaling axis

Although purinergic signaling has been extensively studied in immune cells and tumor cells, very few studies were conducted in adult stem cells under either normal or pathological conditions. An earlier study showed that eATP could promote the proliferation of $CD34^+$ hematopoietic stem cells (HSCs) (Lemoli et al., 2004). eATP was also found to promote mobilization of HSCs from bone marrow to peripheral blood, while eAdo inhibited this process (Adamiak et al., 2018). In addition, both CD150-high bone marrow T-regulatory cells (Tregs) and myeloid progenitors were shown to promote HSC quiescence via eAdo and Ado P1 receptors (Hirata et al., 2018; Umemoto et al., 2018). Here, we investigated the impact of eAdo/eAMP on adult MuSCs in *db/db* diabetic mice. We showed that elevated eAdo/eAMP strongly inhibited activation of QSCs by preventing them from re-entering the cell cycle. Although eAMP was as effective as eAdo in suppressing activation of QSCs, its effect is most likely mediated by Ado with the help of ectonucleotidases like TNAP or CD73 based on the following evidence: first, no AMP-specific membrane-bound receptors are known to exist. Second, both eAMP and eAdo elicited very similar transcriptomic changes in ASCs (Figure S4). Third, the suppressive effect of AMP on MuSCs could be effectively reversed by an ENT inhibitor (Figures S6A and S6B). Mechanistically, we showed that eAdo exerts its inhibitory effect on MuSCs via the ENTs-ADK axis, resulting in increased ratio of intracellular [AMP]/[ATP] and subsequent activation of AMPK. Increased AMPK activity can inhibit mTORC1 via multiple mechanisms: AMPK can phosphorylate Tsc2, which inhibits Rheb by converting it to a GDP-bound form that cannot activate mTORC1. Moreover, AMPK can also directly phosphorylate Raptor, a key component of the mTORC1 complex, to prevent mTORC1 from activating its downstream targets (Liu and Sabatini, 2020). Our recent work showed that mTORC1 is involved in two distinct checkpoints before QSCs re-enter the cell cycle: an early-activation checkpoint involves PI3K with mTORC1 being activated to a lower threshold. It

Figure 6. eAdo/eAMP suppressed mTORC1 via AMPK

(A) FISCs were cultured for 24 h under different conditions as indicated. WCLs were subjected to western blotting. A representative blot is shown.

(B) The relevant band intensity in (A) was quantified by densitometry (n = 3).

(C) FISCs were treated with 0.25 mM AMP in culture for various times. The cellular AMP and ATP levels were measured and the AMP to ATP ratios were calculated and are presented (n = 3).

(D and E) C2C12 cells were serum starved for 4 h followed by treatment with eAMP for 15 min or eAdo for 12 h. WCLs were subjected to western blotting. Representative blots are shown. Quantification was done similarly as described in (B) (n = 5 for D; n = 4 for E).

(F) FISCs were cultured with or without AICAR for 24 h. WCL were subjected to western blotting. A representative blot is shown.

(G) Quantification was done similarly as in (B) (n = 3).

(H) FISCs were cultured with AICAR and EdU for 46 h, followed by cell fixation and staining with EdU (green) and DAPI (blue).

(I) Quantification of the percentage of EdU^+ MuSCs in (H) (n = 3).

Data are presented as mean ± SD.

Scale bar: 50 μm.

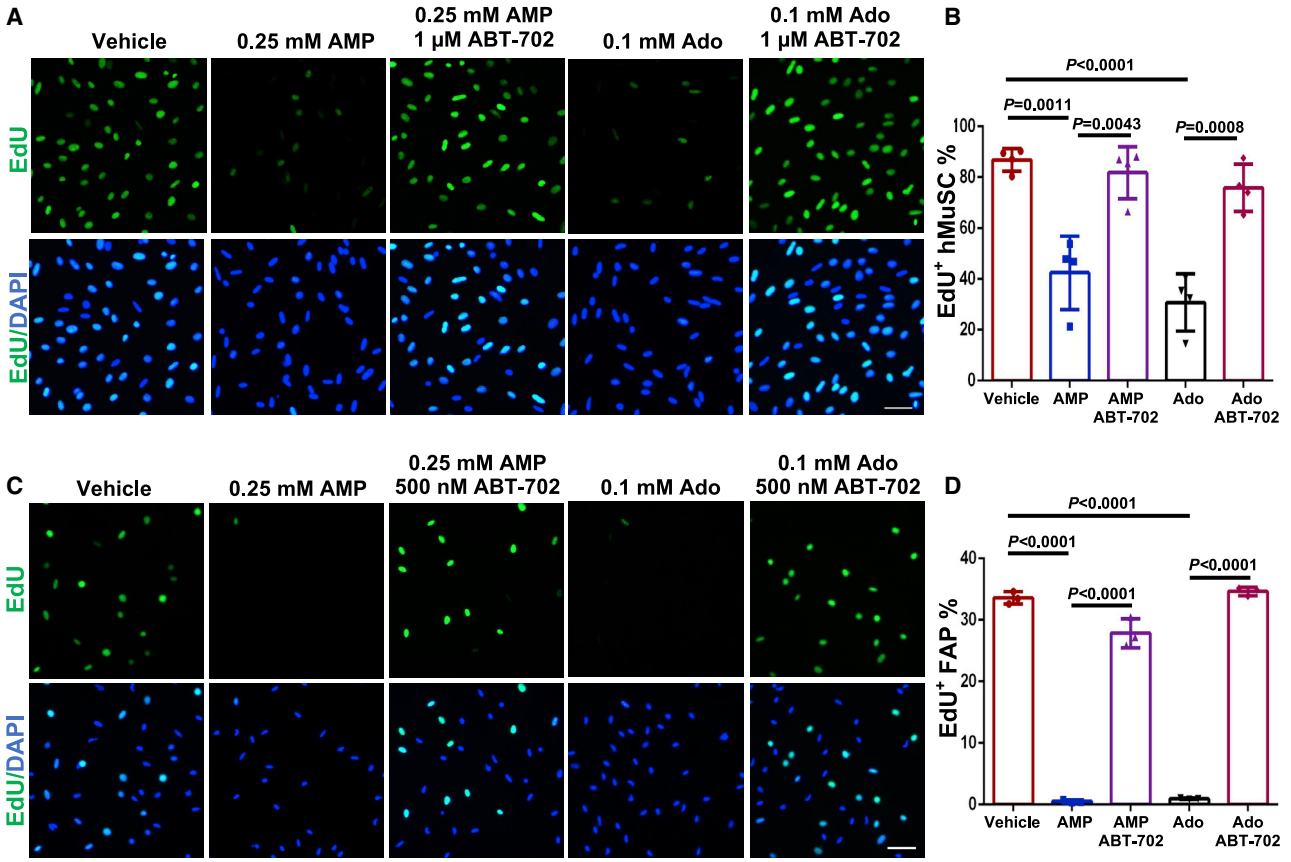

Figure 7. eAdo/eAMP inhibited early activation of human MuSCs and mouse FAPs

(A–D) Freshly isolated human MuSCs (hMuSCs) (A, B) or mouse FAPs (C, D) were cultured with EdU and 0.25 mM eAMP or 0.1 mM eAdo with or without ABT-702 (1 μM for A and 0.5 μM for C) for various times (3 days for A and 2 days for C) followed by cell fixation and staining with EdU (green) and DAPI (blue).

(A and C) Representative fluorescent images. Scale bars: 50 μm.

(B and D) Quantification of the percentage of EdU^+ hMuSCs from (A) (n = 4) and EdU^+ FAPs from (C) (n = 3), respectively. Data were presented as mean ± SD. See also Figure S7.

determines whether QSCs can start the activation process or be awakened (Wang et al., 2018). A late activation checkpoint operates around 16–24 h after injury, with mTORC1 being further activated to a higher threshold to sustain rapid cell growth (Zhou et al., 2021). Defects in either checkpoint block QSCs from re-entering the cell cycle, resulting in a complete regeneration failure (Wang et al., 2018; Zhou et al., 2021). Such a two-tier activation profile for mTORC1 was also seen during activation of naive T cells (also quiescent) in response to co-stimulation of T cell receptor (TCR) and CD28 (Yang et al., 2013). The elevated mTORC1 activity in the late activation checkpoint is likely induced by the nutrient sensing pathway to sustain rapid cell growth before quiescent cells re-enter the cell cycle (Yang et al., 2013; Zhou et al., 2021). We showed that eAdo impairs MuSCs via the ENTs-ADK-AMPK signaling axis by specifically inhibiting the elevated mTORC1 activity at the late cell growth checkpoint (Figures 3H and S5B–S5D). Interestingly, metformin, a first-line drug for diabetes treatment, is known to activate AMPK (Pernicova and Korbonits, 2014). Based on our findings here, the metformin-induced AMPK activation could lead to mTORC1 inhibition in MuSCs, which would impair the functions of MuSCs. Thus, it is likely that long-term metformin uptake may generate undesirable side effects by impairing adult stem cells and tissue regeneration. Consistently, a recent study found that prolonged metformin uptake indeed delayed activation of MuSCs both in culture and *in vivo* (Pavlidou et al., 2019). Moreover, we showed that the inhibitory effect of eAdo is not limited to MuSCs, as activation of quiescent FAPs was also inhibited by eAdo (Figures 7C and 7D). This suggests that eAdo could inhibit multiple quiescent cell types via a conserved mechanism during their transition into the proliferating state. In addition to the impairment of early activation in MuSCs, we found that Ado also impaired myogenic differentiation in culture (our unpublished data), which could partially account for defective muscle regeneration in *db/db* mice *in vivo*. Moreover, we also noticed a decreased pool of QSCs in uninjured *db/db* mice, suggesting defective maintenance of the QSC pool in type 2 diabetic mice (Figures S2B–S2D). Our preliminary study showed that, unlike QSCs from inducible *Rbpj*-KO mice, QSCs from *db/db* mice did not undergo premature activation and differentiation, which

may potentially account for a decreased QSC pool (Bjornson et al., 2012; Mourikis et al., 2012). Instead, cell death is more likely a cause as we detected upregulation of several pro-apoptosis genes (e.g., *p53* and *Bax*) in FISCs from *db*/*db* mice. Nevertheless, using an apoptosis-sensitive cell-permeable probe, we did not detect more apoptotic cells in FISCs from *db*/*db* diabetic mice (our unpublished data). It is likely that QSCs in *db*/*db* mice may die by a non-apoptosis mechanism. Interestingly, a decreased QSC pool was also reported in type 1 diabetic human and mice (D'Souza et al., 2016). It remains to be determined whether elevated eAdo also underlies the decreased QSC pool in both type 1 and type 2 diabetic mice.

ENT inhibitors like dipyridamole are already clinically approved drugs for the treatment of cerebrovascular diseases such as stroke (Chakrabarti and Freedman, 2008). Moreover, dipyridamole was also found to have a protective role in diabetic nephropathy (Elsherbiny et al., 2015). Similarly, inhibition of ADK in diabetic mice was also found to be beneficial: ABT-702 was found to ameliorate diabetic retinopathy (Elsherbiny et al., 2013) and to protect the kidney of STZ-induced diabetic mice (Pye et al., 2014). In addition, ADK inhibition also promotes proliferation of rodent and porcine β cells (Annes et al., 2012). Moreover, genetic disruption of *Adk* in mouse pancreatic β cells protected mice against HFD-induced diabetes (Navarro et al., 2017). However, due to toxicity problems, no ADK inhibitors have been approved for clinical use (Jarvis, 2019). Interestingly, prolonged ADKI treatment was shown to reduce blood glucose levels in diabetic mice (Annes et al., 2012; Elsherbiny et al., 2013; Navarro et al., 2017; Pye et al., 2014), which was also confirmed by us (Figure S6I). Importantly, ABT-702 treatment of *db*/*db* mice mitigated the adverse effect of eAdo on MuSC activation *in vivo* (Figures 5E–5G). Due to the conserved nature of the eAdo-ENTs-ADK signaling axis in both mouse and human MuSCs, both ENTs and ADK may serve as promising therapeutic targets for restoring the regenerative potentials of adult stem/progenitor cells in patients with diabetes.

Limitations of the study

Although our current study mainly focused on the impact of elevated eAdo and eAMP on quiescent MuSCs in *db*/*db* diabetic mice, other diabetes-associated pathogenic mechanisms, including oxidative stress, chronic inflammation, and altered metabolism and signaling pathways, could also impair the functions of MuSCs. Moreover, dysfunctional vasculature and altered immune systems that are commonly associated with diabetes could also impede muscle regeneration as both endothelial cells of the vasculature and various immune cells are present in injured muscles and known to interact with MuSCs during the regeneration process. Furthermore, due to the broad expression of ENTs and adenosine receptors, eAdo could also exert its effect on other cell types (e.g., immune cells, FAPs, and endothelial cells). Therefore, our current study only represents a defined pathogenic mechanism by which eAdo impairs MuSCs and muscle regeneration. In the future, it will be important to elucidate whether different pathogenic mechanisms are intrinsically connected or act independently to impair tissue regeneration in diabetes.

STAR★METHODS

Detailed methods are provided in the online version of this paper and include the following:

- KEY RESOURCES TABLE
- RESOURCE AVAILABILITY
  - Lead contact
  - Materials availability
  - Data and code availability
- EXPERIMENTAL MODEL AND SUBJECT DETAILS
  - Animals
  - Human skeletal muscle biopsies
- METHOD DETAILS
  - Isolation of MuSCs by fluorescence-activated cell sorting (FACS)
  - Isolation of single myofibers
  - Muscle injury by cardiotoxin (CTX) or $BaCl_2$ injection
  - Hematoxylin and eosin (H&E) staining
  - Immunostaining
  - Western blot
  - EdU labelling
  - The AMP/ATP assay
  - The Seahorse Cell Mito Stress assay
  - RNA-seq and data processing
- QUANTIFICATION AND STATISTICAL ANALYSIS
  - Image quantification
  - Statistical analysis

SUPPLEMENTAL INFORMATION

Supplemental information can be found online at https://doi.org/10.1016/j.celrep.2022.110884.

ACKNOWLEDGMENTS

The project was supported by research grants from the Hong Kong Research Grant Council (N_HKUST633/18, C6018-19G, AoE/M-09/12, AoE/M-604/16, T13-602/21-N, and T13-605/18-W), the State Key Laboratory of Molecular Neuroscience at HKUST, the Hong Kong Center for Neurodegenerative Diseases (HKCeND), the National Natural Science Foundation of China (31861163004), and the Shenzhen Bay Laboratory (S201101002, Guangdong, China).

AUTHOR CONTRIBUTIONS

Z.W. and J.Z. conceived the project. L.H. and Z.W. designed experiments, analyzed data, and wrote the manuscript. L.H. performed the experiments with the help of G.W., S.Z., C.S., and Y.Q. Y.H. and A.X. provided diabetic mice-related reagents, protocols, and advice. M.T.Y.O. provided human muscle biopsies. Z.H., Y.L., and H.W. helped with human MuSC isolation. All authors contributed to data analysis and manuscript editing.

DECLARATION OF INTERESTS

The authors declare no competing interests.

Received: August 17, 2021
Revised: April 12, 2022
Accepted: May 5, 2022
Published: May 31, 2022

REFERENCES

Adamiak, M., Bujko, K., Cymer, M., Plonka, M., Glaser, T., Kucia, M., Ratajczak, J., Ulrich, H., Abdel-Latif, A., and Ratajczak, M.Z. (2018). Novel evidence that extracellular nucleotides and purinergic signaling induce innate immunity-mediated mobilization of hematopoietic stem/progenitor cells. Leukemia *32*, 1920–1931. https://doi.org/10.1038/s41375-018-0122-0.

d'Albis, A., Couteaux, R., Janmot, C., Roulet, A., and Mira, J.C. (1988). Regeneration after cardiotoxin injury of innervated and denervated slow and fast muscles of mammals. Myosin isoform analysis. Eur. J. Biochem. *174*, 103–110. https://doi.org/10.1111/j.1432-1033.1988.tb14068.x.

Allard, B., Allard, D., Buisseret, L., and Stagg, J. (2020). The adenosine pathway in immuno-oncology. Nat. Rev. Clin. Oncol. *17*, 611–629. https://doi.org/10.1038/s41571-020-0382-2.

Annes, J.P., Ryu, J.H., Lam, K., Carolan, P.J., Utz, K., Hollister-Lock, J., Arvanites, A.C., Rubin, L.L., Weir, G., and Melton, D.A. (2012). Adenosine kinase inhibition selectively promotes rodent and porcine islet β-cell replication. Proc. Natl. Acad. Sci. U S A *109*, 3915–3920. https://doi.org/10.1073/pnas.1201149109.

Antonioli, L., Blandizzi, C., Pacher, P., and Haskó, G. (2013). Immunity, inflammation and cancer: a leading role for adenosine. Nat. Rev. Cancer *13*, 842–857. https://doi.org/10.1038/nrc3613.

Antonioli, L., Blandizzi, C., Csóka, B., Pacher, P., and Haskó, G. (2015). Adenosine signalling in diabetes mellitus—pathophysiology and therapeutic considerations. Nat. Rev. Endocrinol. *11*, 228–241. https://doi.org/10.1038/nrendo.2015.10.

Arounleut, P., Bowser, M., Upadhyay, S., Shi, X.-M., Fulzele, S., Johnson, M.H., Stranahan, A.M., Hill, W.D., Isales, C.M., and Hamrick, M.W. (2013). Absence of functional leptin receptor isoforms in the POUND (Leprdb/lb) mouse is associated with muscle atrophy and altered myoblast proliferation and differentiation. PLoS One *8*, e72330. https://doi.org/10.1371/journal.pone.0072330.

Baghdadi, M.B., and Tajbakhsh, S. (2018). Regulation and phylogeny of skeletal muscle regeneration. Dev. Biol. *433*, 200–209. https://doi.org/10.1016/j.ydbio.2017.07.026.

Baghdadi, M.B., Castel, D., Machado, L., Fukada, S., Birk, D.E., Relaix, F., Tajbakhsh, S., and Mourikis, P. (2018). Notch/CollagenV/CalcR reciprocal signalling retains muscle stem cells in their niche. Nature *557*, 714–718.

Bentzinger, C.F., Wang, Y.X., von Maltzahn, J., Soleimani, V.D., Yin, H., and Rudnicki, M.A. (2013). Fibronectin regulates Wnt7a signaling and satellite cell expansion. Cell Stem Cell *12*, 75–87. https://doi.org/10.1016/j.stem.2012.09.015.

Bjornson, C.R.R., Cheung, T.H., Liu, L., Tripathi, P.V., Steeper, K.M., and Rando, T.A. (2012). Notch signaling is necessary to maintain quiescence in adult muscle stem cells. Stem Cells Dayt. Ohio *30*, 232–242. https://doi.org/10.1002/stem.773.

Boison, D., and Yegutkin, G.G. (2019). Adenosine metabolism: emerging concepts for cancer therapy. Cancer Cell *36*, 582–596. https://doi.org/10.1016/j.ccell.2019.10.007.

Burnstock, G. (2012). Discovery of purinergic signalling, the initial resistance and current explosion of interest. Br. J. Pharmacol. *167*, 238–255. https://doi.org/10.1111/j.1476-5381.2012.02008.x.

Burnstock, G. (2016). An introduction to the roles of purinergic signalling in neurodegeneration, neuroprotection and neuroregeneration. Neuropharmacology *104*, 4–17. https://doi.org/10.1016/j.neuropharm.2015.05.031.

Ceddia, R.B. (2005). Direct metabolic regulation in skeletal muscle and fat tissue by leptin: implications for glucose and fatty acids homeostasis. Int. J. Obes. *29*, 1175–1183. https://doi.org/10.1038/sj.ijo.0803025.

Cekic, C., and Linden, J. (2016). Purinergic regulation of the immune system. Nat. Rev. Immunol. *16*, 177–192. https://doi.org/10.1038/nri.2016.4.

Chakrabarti, S., and Freedman, J.E. (2008). Dipyridamole, cerebrovascular disease, and the vasculature. Vascul. Pharmacol. *48*, 143–149. https://doi.org/10.1016/j.vph.2007.12.004.

Charville, G.W., Cheung, T.H., Yoo, B., Santos, P.J., Lee, G.K., Shrager, J.B., and Rando, T.A. (2015). Ex vivo expansion and in vivo self-renewal of human muscle stem cells. Stem Cell Rep. *5*, 621–632. https://doi.org/10.1016/j.stemcr.2015.08.004.

Cole, J.B., and Florez, J.C. (2020). Genetics of diabetes mellitus and diabetes complications. Nat. Rev. Nephrol. *16*, 377–390. https://doi.org/10.1038/s41581-020-0278-5.

Corcoran, M.P., Lamon-Fava, S., and Fielding, R.A. (2007). Skeletal muscle lipid deposition and insulin resistance: effect of dietary fatty acids and exercise. Am. J. Clin. Nutr. *85*, 662–677. https://doi.org/10.1093/ajcn/85.3.662.

Cronstein, B.N., and Sitkovsky, M. (2017). Adenosine and adenosine receptors in the pathogenesis and treatment of rheumatic diseases. Nat. Rev. Rheumatol. *13*, 41–51. https://doi.org/10.1038/nrrheum.2016.178.

Di Virgilio, F., and Adinolfi, E. (2017). Extracellular purines, purinergic receptors and tumor growth. Oncogene *36*, 293–303. https://doi.org/10.1038/onc.2016.206.

Di Virgilio, F., Dal Ben, D., Sarti, A.C., Giuliani, A.L., and Falzoni, S. (2017). The P2X7 receptor in infection and inflammation. Immunity *47*, 15–31. https://doi.org/10.1016/j.immuni.2017.06.020.

Dosch, M., Gerber, J., Jebbawi, F., and Beldi, G. (2018). Mechanisms of ATP release by inflammatory cells. Int. J. Mol. Sci. *19*, 1222. https://doi.org/10.3390/ijms19041222.

D'Souza, D.M., Zhou, S., Rebalka, I.A., MacDonald, B., Moradi, J., Krause, M.P., Al-Sajee, D., Punthakee, Z., Tarnopolsky, M.A., and Hawke, T.J. (2016). Decreased satellite cell number and function in humans and mice with type 1 diabetes is the result of altered Notch signaling. Diabetes *65*, 3053–3061. https://doi.org/10.2337/db15-1577.

Dudzinska, W. (2014). Purine nucleotides and their metabolites in patients with type 1 and 2 diabetes mellitus. J. Biomed. Sci. Eng. *07*, 38–44. https://doi.org/10.4236/jbise.2014.71006.

Elsherbiny, N.M., Ahmad, S., Naime, M., Elsherbini, A.M., Fulzele, S., Al-Gayyar, M.M., Eissa, L.A., El-Shishtawy, M.M., and Liou, G.I. (2013). ABT-702, an adenosine kinase inhibitor, attenuates inflammation in diabetic retinopathy. Life Sci. *93*, 78–88. https://doi.org/10.1016/j.lfs.2013.05.024.

Elsherbiny, N.M., Al-Gayyar, M.M.H., and Abd El Galil, K.H. (2015). Nephroprotective role of dipyridamole in diabetic nephropathy: effect on inflammation and apoptosis. Life Sci. *143*, 8–17. https://doi.org/10.1016/j.lfs.2015.10.026.

Evano, B., and Tajbakhsh, S. (2018). Skeletal muscle stem cells in comfort and stress. Npj Regen. Med. *3*, 24. https://doi.org/10.1038/s41536-018-0062-3.

Faas, M.M., Sáez, T., and de Vos, P. (2017). Extracellular ATP and adenosine: the Yin and Yang in immune responses? Mol. Aspects Med. *55*, 9–19. https://doi.org/10.1016/j.mam.2017.01.002.

Fu, X., Zhu, M., Zhang, S., Foretz, M., Viollet, B., and Du, M. (2016). Obesity impairs skeletal muscle regeneration through inhibition of AMPK. Diabetes *65*, 188–200. https://doi.org/10.2337/db15-0647.

Fuchs, E., and Blau, H.M. (2020). Tissue stem cells: architects of their niches. Cell Stem Cell *27*, 532–556. https://doi.org/10.1016/j.stem.2020.09.011.

Garcia, D., and Shaw, R.J. (2017). AMPK: mechanisms of cellular energy sensing and restoration of metabolic balance. Mol. Cell *66*, 789–800. https://doi.org/10.1016/j.molcel.2017.05.032.

García-Prat, L., Perdiguero, E., Alonso-Martín, S., Dell'Orso, S., Ravichandran, S., Brooks, S.R., Juan, A.H., Campanario, S., Jiang, K., Hong, X., et al. (2020). FoxO maintains a genuine muscle stem-cell quiescent state until geriatric age. Nat. Cell Biol. *22*, 1307–1318. https://doi.org/10.1038/s41556-020-00593-7.

Hirata, Y., Furuhashi, K., Ishii, H., Li, H.W., Pinho, S., Ding, L., Robson, S.C., Frenette, P.S., and Fujisaki, J. (2018). CD150high bone marrow Tregs maintain hematopoietic stem cell quiescence and immune privilege via adenosine. Cell Stem Cell *22*, 445–453.e5. https://doi.org/10.1016/j.stem.2018.01.017.

Holtzman, S.G. (1996). Discriminative effects of CGS 15943, a competitive adenosine receptor antagonist, in monkeys: comparison to methylxanthines. J. Pharmacol. Exp. Ther. *277*, 739–746.

Huang, Z., Xie, N., Illes, P., Di Virgilio, F., Ulrich, H., Semyanov, A., Verkhratsky, A., Sperlagh, B., Yu, S.-G., Huang, C., et al. (2021). From purines to purinergic

signalling: molecular functions and human diseases. Signal. Transduct. Target. Ther. *6*, 162. https://doi.org/10.1038/s41392-021-00553-z.

Idzko, M., Ferrari, D., Riegel, A.-K., and Eltzschig, H.K. (2014). Extracellular nucleotide and nucleoside signaling in vascular and blood disease. Blood *124*, 1029–1037. https://doi.org/10.1182/blood-2013-09-402560.

Jarvis, M.F. (2019). Therapeutic potential of adenosine kinase inhibition-Revisited. Pharmacol. Res. Perspect. *7*, e00506. https://doi.org/10.1002/prp2.506.

Jarvis, M.F., Yu, H., Kohlhaas, K., Alexander, K., Lee, C.H., Jiang, M., Bhagwat, S.S., Williams, M., and Kowaluk, E.A. (2000). ABT-702 (4-amino-5-(3-bromophenyl)-7-(6-morpholinopyridin-3-yl)pyrido[2, 3-d]pyrimidine), a novel orally effective adenosine kinase inhibitor with analgesic and anti-inflammatory properties: I. In vitro characterization and acute antinociceptive effects in the mouse. J. Pharmacol. Exp. Ther. *295*, 1156–1164.

Joe, A.W.B., Yi, L., Natarajan, A., Le Grand, F., So, L., Wang, J., Rudnicki, M.A., and Rossi, F.M.V. (2010). Muscle injury activates resident fibro/adipogenic progenitors that facilitate myogenesis. Nat. Cell Biol. *12*, 153–163. https://doi.org/10.1038/ncb2015.

Johansson, S.M., Salehi, A., Sandström, M.E., Westerblad, H., Lundquist, I., Carlsson, P.-O., Fredholm, B.B., and Katz, A. (2007). A1 receptor deficiency causes increased insulin and glucagon secretion in mice. Biochem. Pharmacol. *74*, 1628–1635. https://doi.org/10.1016/j.bcp.2007.08.006.

Kleinert, M., Clemmensen, C., Hofmann, S.M., Moore, M.C., Renner, S., Woods, S.C., Huypens, P., Beckers, J., de Angelis, M.H., Schürmann, A., et al. (2018). Animal models of obesity and diabetes mellitus. Nat. Rev. Endocrinol. *14*, 140–162. https://doi.org/10.1038/nrendo.2017.161.

Lemoli, R.M., Ferrari, D., Fogli, M., Rossi, L., Pizzirani, C., Forchap, S., Chiozzi, P., Vaselli, D., Bertolini, F., Foutz, T., et al. (2004). Extracellular nucleotides are potent stimulators of human hematopoietic stem cells in vitro and in vivo. Blood *104*, 1662–1670. https://doi.org/10.1182/blood-2004-03-0834.

Li, L., Rozo, M., Yue, S., Zheng, X., Tan, F.J., Lepper, C., and Fan, C.-M. (2019). Muscle stem cell renewal suppressed by GAS1 can be reversed by GDNF in mice. Nat. Metab. *1*, 985–995. https://doi.org/10.1038/s42255-019-0110-3.

Liu, G.Y., and Sabatini, D.M. (2020). mTOR at the nexus of nutrition, growth, ageing and disease. Nat. Rev. Mol. Cell Biol. *21*, 183–203. https://doi.org/10.1038/s41580-019-0199-y.

Lukjanenko, L., Jung, M.J., Hegde, N., Perruisseau-Carrier, C., Migliavacca, E., Rozo, M., Karaz, S., Jacot, G., Schmidt, M., Li, L., et al. (2016). Loss of fibronectin from the aged stem cell niche affects the regenerative capacity of skeletal muscle in mice. Nat. Med. *22*, 897–905. https://doi.org/10.1038/nm.4126.

Machado, L., Esteves de Lima, J., Fabre, O., Proux, C., Legendre, R., Szegedi, A., Varet, H., Ingerslev, L.R., Barrès, R., Relaix, F., et al. (2017). In situ fixation redefines quiescence and early activation of skeletal muscle stem cells. Cell Rep. *21*, 1982–1993. https://doi.org/10.1016/j.celrep.2017.10.080.

Machado, L., Geara, P., Camps, J., Dos Santos, M., Teixeira-Clerc, F., Van Herck, J., Varet, H., Legendre, R., Pawlotsky, J.-M., Sampaolesi, M., et al. (2021). Tissue damage induces a conserved stress response that initiates quiescent muscle stem cell activation. Cell Stem Cell *28*, 1125–1135.e7. https://doi.org/10.1016/j.stem.2021.01.017.

Mourikis, P., Sambasivan, R., Castel, D., Rocheteau, P., Bizzarro, V., and Tajbakhsh, S. (2012). A critical requirement for Notch signaling in maintenance of the quiescent skeletal muscle stem cell state. Stem Cells *30*, 243–252. https://doi.org/10.1002/stem.775.

Navarro, G., Abdolazimi, Y., Zhao, Z., Xu, H., Lee, S., Armstrong, N.A., and Annes, J.P. (2017). Genetic disruption of adenosine kinase in mouse pancreatic β-cells protects against high-fat diet–induced glucose intolerance. Diabetes *66*, 1928–1938. https://doi.org/10.2337/db16-0816.

Németh, Z.H., Bleich, D., Csóka, B., Pacher, P., Mabley, J.G., Himer, L., Vizi, E.S., Deitch, E.A., Szabó, C., Cronstein, B.N., et al. (2007). Adenosine receptor activation ameliorates type 1 diabetes. FASEB J *21*, 2379–2388. https://doi.org/10.1096/fj.07-8213com.

Nguyen, M.-H., Cheng, M., and Koh, T.J. (2011). Impaired muscle regeneration in ob/ob and db/db mice. ScientificWorldJournal *11*, 1525–1535. https://doi.org/10.1100/tsw.2011.137.

Pardo, F., Villalobos-Labra, R., Chiarello, D.I., Salsoso, R., Toledo, F., Gutierrez, J., Leiva, A., and Sobrevia, L. (2017). Molecular implications of adenosine in obesity. Mol. Aspects Med. *55*, 90–101. https://doi.org/10.1016/j.mam.2017.01.003.

Pastor-Anglada, M., and Pérez-Torras, S. (2018). Who is who in adenosine transport. Front. Pharmacol. *9*, 627. https://doi.org/10.3389/fphar.2018.00627.

Pavlidou, T., Marinkovic, M., Rosina, M., Fuoco, C., Vumbaca, S., Gargioli, C., Castagnoli, L., and Cesareni, G. (2019). Metformin delays satellite cell activation and maintains quiescence. Stem Cells Int. *2019*, e5980465. https://doi.org/10.1155/2019/5980465.

Peleli, M., and Carlstrom, M. (2017). Adenosine signaling in diabetes mellitus and associated cardiovascular and renal complications. Mol. Aspects Med. *55*, 62–74. https://doi.org/10.1016/j.mam.2016.12.001.

Pernicova, I., and Korbonits, M. (2014). Metformin–mode of action and clinical implications for diabetes and cancer. Nat. Rev. Endocrinol. *10*, 143–156. https://doi.org/10.1038/nrendo.2013.256.

Picelli, S., Faridani, O.R., Björklund, A.K., Winberg, G., Sagasser, S., and Sandberg, R. (2014). Full-length RNA-seq from single cells using Smart-seq2. Nat. Protoc. *9*, 171–181. https://doi.org/10.1038/nprot.2014.006.

Pye, C., Elsherbiny, N.M., Ibrahim, A.S., Liou, G.I., Chadli, A., Al-Shabrawey, M., and Elmarakby, A.A. (2014). Adenosine kinase inhibition protects the kidney against streptozotocin-induced diabetes through anti-inflammatory and anti-oxidant mechanisms. Pharmacol. Res. *85*, 45–54. https://doi.org/10.1016/j.phrs.2014.05.004.

Relaix, F., Bencze, M., Borok, M.J., Der Vartanian, A., Gattazzo, F., Mademtzoglou, D., Perez-Diaz, S., Prola, A., Reyes-Fernandez, P.C., Rotini, A., et al. (2021). Perspectives on skeletal muscle stem cells. Nat. Commun. *12*, 692. https://doi.org/10.1038/s41467-020-20760-6.

Ritchie, R.H., and Abel, E.D. (2020). Basic mechanisms of diabetic heart disease. Circ. Res. *126*, 1501–1525. https://doi.org/10.1161/circresaha.120.315913.

Rocheteau, P., Gayraud-Morel, B., Siegl-Cachedenier, I., Blasco, M.A., and Tajbakhsh, S. (2012). A subpopulation of adult skeletal muscle stem cells retains all template DNA strands after cell division. Cell *148*, 112–125. https://doi.org/10.1016/j.cell.2011.11.049.

Rodgers, J.T., King, K.Y., Brett, J.O., Cromie, M.J., Charville, G.W., Maguire, K.K., Brunson, C., Mastey, N., Liu, L., Tsai, C.-R., et al. (2014). mTORC1 controls the adaptive transition of quiescent stem cells from G 0 to G Alert. Nature *510*, 393–396. https://doi.org/10.1038/nature13255.

Rossi, L., Salvestrini, V., Ferrari, D., Di Virgilio, F., and Lemoli, R.M. (2012). The sixth sense: hematopoietic stem cells detect danger through purinergic signaling. Blood *120*, 2365–2375. https://doi.org/10.1182/blood-2012-04-422378.

Stone, T.W., Ceruti, S., and Abbracchio, M.P. (2009). Adenosine receptors and neurological disease: neuroprotection and neurodegeneration. Handb. Exp. Pharmacol., 535–587. https://doi.org/10.1007/978-3-540-89615-9_17.

Subramanian, A., Tamayo, P., Mootha, V.K., Mukherjee, S., Ebert, B.L., Gillette, M.A., Paulovich, A., Pomeroy, S.L., Golub, T.R., Lander, E.S., et al. (2005). Gene set enrichment analysis: a knowledge-based approach for interpreting genome-wide expression profiles. Proc. Natl. Acad. Sci. *102*, 15545–15550. https://doi.org/10.1073/pnas.0506580102.

Towler, M.C., and Hardie, D.G. (2007). AMP-activated protein kinase in metabolic control and insulin signaling. Circ. Res. *100*, 328–341. https://doi.org/10.1161/01.res.0000256090.42690.05.

Uezumi, A., Nakatani, M., Ikemoto-Uezumi, M., Yamamoto, N., Morita, M., Yamaguchi, A., Yamada, H., Kasai, T., Masuda, S., Narita, A., et al. (2016). Cell-surface protein profiling identifies distinctive markers of progenitor cells in human skeletal muscle. Stem Cell Rep. *7*, 263–278. https://doi.org/10.1016/j.stemcr.2016.07.004.

Umemoto, T., Hashimoto, M., Matsumura, T., Nakamura-Ishizu, A., and Suda, T. (2018). Ca2+-mitochondria axis drives cell division in hematopoietic stem cells. J. Exp. Med. *215*, 2097–2113. https://doi.org/10.1084/jem.20180421.

Varadaiah, Y.G.C., Sivanesan, S., Nayak, S.B., and Thirumalarao, K.R. (2019). Purine metabolites can indicate diabetes progression. Arch. Physiol. Biochem. *128*, 87–91. https://doi.org/10.1080/13813455.2019.1663219.

van Velthoven, C.T.J., and Rando, T.A. (2019). Stem cell quiescence: dynamism, restraint, and cellular idling. Cell Stem Cell *24*, 213–225. https://doi.org/10.1016/j.stem.2019.01.001.

van Velthoven, C.T.J., de Morree, A., Egner, I.M., Brett, J.O., and Rando, T.A. (2017). Transcriptional profiling of quiescent muscle stem cells in vivo. Cell Rep. *21*, 1994–2004. https://doi.org/10.1016/j.celrep.2017.10.037.

Wang, G., Zhu, H., Situ, C., Han, L., Yu, Y., Cheung, T.H., Liu, K., and Wu, Z. (2018). p110α of PI3K is necessary and sufficient for quiescence exit in adult muscle satellite cells. EMBO J. *37*, e98239. https://doi.org/10.15252/embj.201798239.

Xia, L., Wang, Z., Zhang, Y., Yang, X., Zhan, Y., Cheng, R., Wang, S., and Zhang, J. (2015). Reciprocal regulation of insulin and plasma 5'-AMP in glucose homeostasis in mice. J. Endocrinol. *224*, 225–234. https://doi.org/10.1530/joe-14-0501.

Xiang, L., Zhang, H., Wei, J., Tian, X.Y., Luan, H., Li, S., Zhao, H., Cao, G., Chung, A.C.K., Yang, C., et al. (2018). Metabolomics studies on db/db diabetic mice in skeletal muscle reveal effective clearance of overloaded intermediates by exercise. Anal. Chim. Acta *1037*, 130–139. https://doi.org/10.1016/j.aca.2017.11.082.

Yang, K., Shrestha, S., Zeng, H., Karmaus, P.W.F., Neale, G., Vogel, P., Guertin, D.A., Lamb, R.F., and Chi, H. (2013). T cell exit from quiescence and differentiation into Th2 cells depend on Raptor-mTORC1-mediated metabolic reprogramming. Immunity *39*, 1043–1056. https://doi.org/10.1016/j.immuni.2013.09.015.

Yang, X., Zhao, Y., Sun, Q., Yang, Y., Gao, Y., Ge, W., Liu, J., Xu, X., Weng, D., Wang, S., et al. (2019a). Adenine nucleotide-mediated regulation of hepatic PTP1B activity in mouse models of type 2 diabetes. Diabetologia *62*, 2106–2117. https://doi.org/10.1007/s00125-019-04971-1.

Yang, X., Zhao, Y., Sun, Q., Yang, Y., Gao, Y., Ge, W., Liu, J., Xu, X., and Zhang, J. (2019b). An intermediary role of adenine nucleotides on free fatty acids-induced hyperglycemia in obese mice. Front. Endocrinol. *10*, 497. https://doi.org/10.3389/fendo.2019.00497.

Yao, S.Y., Ng, A.M., Muzyka, W.R., Griffiths, M., Cass, C.E., Baldwin, S.A., and Young, J.D. (1997). Molecular cloning and functional characterization of nitrobenzylthioinosine (NBMPR)-sensitive (es) and NBMPR-insensitive (ei) equilibrative nucleoside transporter proteins (rENT1 and rENT2) from rat tissues. J. Biol. Chem. *272*, 28423–28430. https://doi.org/10.1074/jbc.272.45.28423.

Yin, H., Price, F., and Rudnicki, M.A. (2013). Satellite cells and the muscle stem cell niche. Physiol. Rev. *93*, 23–67. https://doi.org/10.1152/physrev.00043.2011.

Yue, F., Bi, P., Wang, C., Shan, T., Nie, Y., Ratliff, T.L., Gavin, T.P., and Kuang, S. (2017). Pten is necessary for the quiescence and maintenance of adult muscle stem cells. Nat. Commun. *8*, 14328. https://doi.org/10.1038/ncomms14328.

Zhang, Y., Dai, Y., Wen, J., Zhang, W., Grenz, A., Sun, H., Tao, L., Lu, G., Alexander, D.C., Milburn, M.V., et al. (2011). Detrimental effects of adenosine signaling in sickle cell disease. Nat. Med. *17*, 79–86. https://doi.org/10.1038/nm.2280.

Zhang, Y., Wang, Z., Zhao, Y., Zhao, M., Wang, S., Hua, Z., and Zhang, J. (2012). The plasma 5′-AMP acts as a potential upstream regulator of hyperglycemia in type 2 diabetic mice. Am. J. Physiol.-Endocrinol. Metab. *302*, E325–E333. https://doi.org/10.1152/ajpendo.00424.2011.

Zheng, Y., Ley, S.H., and Hu, F.B. (2018). Global aetiology and epidemiology of type 2 diabetes mellitus and its complications. Nat. Rev. Endocrinol. *14*, 88–98. https://doi.org/10.1038/nrendo.2017.151.

Zhou, S., Han, L., Weng, M., Zhu, H., Heng, Y., Wang, G., Shen, Z., Chen, X., Fu, X., Zhang, M., et al. (2021). Paxbp1 controls a key checkpoint for cell growth and survival during early activation of quiescent muscle satellite cells. Proc. Natl. Acad. Sci. U. S. A. *118*, e2021093118. https://doi.org/10.1073/pnas.2021093118.

STAR★METHODS

KEY RESOURCES TABLE

REAGENT or RESOURCE	SOURCE	IDENTIFIER
Antibodies		
Rabbit polyclonal anti-MyoD	Santa Cruz Biotechnology	Cat# sc-760; RRID: AB_2148870
Mouse monoclonal anti-Myogenin	Santa Cruz Biotechnology	Cat# sc-12732; RRID: AB_627980
Rabbit polyclonal anti-Tomm20	Santa Cruz Biotechnology	Cat# sc-11415; RRID: AB_2207533
Rabbit monoclonal anti-p-S6 (S235/236)	Cell Signaling Technology	Cat# 4858L; RRID: AB_916156
Rabbit monoclonal anti-S6	Cell Signaling Technology	Cat# 2217S; RRID: AB_331355
Rabbit monoclonal anti-p-4E-BP1 (T37/46)	Cell Signaling Technology	Cat# 2855S; RRID: AB_560835
Rabbit polyclonal anti-4E-BP1	Cell Signaling Technology	Cat# 9452S; RRID: AB_331692
Rabbit monoclonal anti-p-AMPKα (T172)	Cell Signaling Technology	Cat# 2535S; RRID: AB_331250
Rabbit polyclonal anti-AMPKα	Cell Signaling Technology	Cat# 2532S; RRID: AB_330331
Rat monoclonal anti-CD34	eBioscience™	Cat# 14-0341-82; RRID: AB_467210
Rabbit polyclonal anti-Laminin	Sigma-Aldrich	Cat# L9393; RRID: AB_477163
Rabbit polyclonal anti-PGC1β	Proteintech	Cat# 22378-1-AP; RRID: AB_2879093
Mouse monoclonal anti-Gapdh	Ambion	Cat# AM4300; RRID: AB_437392
Mouse monoclonal anti-Myosin heavy chain, sarcomere (MHC)	Developmental Studies Hybridoma Bank	Cat# MF20; RRID: AB_2147781
Mouse monoclonal anti-Myosin heavy chain (embryonic)	Developmental Studies Hybridoma Bank	Cat# F1.652-s; RRID: AB_528358
Mouse monoclonal anti-Pax7	Developmental Studies Hybridoma Bank	Cat# pax7; RRID: AB_528428
Goat anti-Mouse IgG H&L Secondary antibody, HRP	Thermo Fisher	Cat# 31430; RRID: AB_228307
Goat anti-Rabbit IgG H&L Secondary antibody, HRP	Thermo Fisher	Cat# 32460; RRID: AB_1185567
Alexa Fluor® 647 anti-mouse Ly-6A/E (Sca1)	BioLegend	Cat# 108118; RRID: AB_493271
FITC anti-mouse CD31	BioLegend	Cat# 102506; RRID: AB_312913
FITC anti-mouse CD45	BioLegend	Cat# 103108; RRID: AB_312973
Biotin anti-mouse CD106 (VCAM-1)	BioLegend	Cat# 105704; RRID: AB_313205
PE/Cyanine7 Streptavidin	BioLegend	Cat# 405206
Alexa Fluor® 488 anti-human CD31	BioLegend	Cat# 303110; RRID: AB_493074
Alexa Fluor® 488 anti-human CD45	Life Technologies	Cat# MHCD4520; RRID: AB_10392555
FITC anti-human CD34	BioLegend	Cat# 343504; RRID: AB_1731852
APC anti-human CD29 (ITGB1)	BioLegend	Cat# 303008; RRID: AB_314324
Biotin anti-human CD56 (NCAM)	BioLegend	Cat# 318320; RRID: AB_893390
PE Streptavidin	BD Biosciences	Cat# 554061; RRID: AB_10053328
Biological samples		
Human skeletal muscle biopsies	The Prince of Wales Hospital (Shatin, Hong Kong)	N/A
Chemicals, peptides, and recombinant proteins		
Dipyridamole	Santa Cruz	Cat# sc-200717
ABT-702	Santa Cruz	Cat# sc-202900
CGS15943	Santa Cruz	Cat# sc-203544
5-Iodotubercidin	Santa Cruz	Cat# sc-3531
P1, P5-Di (adenosine-5'-) pentaphosphate, Trilithium salt	Santa Cruz	Cat# sc-204156
Pentostatin	AdooQ Bioscience	Cat# A11534-10
Cpd3	Calbiochem	Cat# 5.33642.0001

(*Continued on next page*)

Continued

REAGENT or RESOURCE	SOURCE	IDENTIFIER
Streptozotocin	Cayman Chemical	Item No. 13104
Carbonyl cyanide 4-(trifluoromethoxy) phenylhydrazone (FCCP)	Santa Cruz	Cat# sc-203578
Oligomycin	Santa Cruz	Cat# sc-203342
Rotenone	Santa Cruz	Cat# sc-203242
Antimycin A	Santa Cruz	Cat# sc-202467
Cardiotoxin	Latoxan Laboratory	Cat# L8102
Critical commercial assays		
Click-iT EdU Cell Proliferation Kit	Thermo Fisher	Cat# C10337
ATP/ADP/AMP Assay Kit	Biomedical Research Service & Clinical Application	Cat# A-125
Deposited data		
RNA-seq of DMSO, AMP or Adenosine treated MuSCs	This paper	GSE175786
Experimental models: Cell lines		
C2C12 cell line	ATCC	CRL-1772
Experimental models: Organisms/strains		
BKS.Cg-Dock7^{m}+/+Lepr^{db}/J	The Jackson Laboratory	Stock No: 000642
B6.129S4-*Pten*$^{tm1Hwu/}$J	The Jackson Laboratory	Stock No: 006440
B6.Cg-Pax7$^{tm1(cre/ERT2)Gaka}$/J :: B6.129X1-Gt(ROSA)26Sor$^{tm1(EYFP)Cos}$/J	(Zhou et al., 2021)	N/A
Software and algorithms		
Fiji (ImageJ)	National Institutes of Health	RRID: SCR_002285
CellProfiler Image Analysis Software	Broad Institute	RRID: SCR_007358
GraphPad Prism (v8)	Graphpad Software	RRID: SCR_002798

RESOURCE AVAILABILITY

Lead contact

Further information and requests for resources and reagents should be directed to and will be fulfilled by the lead contact, Zhenguo Wu (bczgwu@ust.hk).

Materials availability

This study did not generate unique reagents.

Data and code availability

All raw and processed RNA-seq data have been deposited at GEO (GEO: GSE175786). Other data are available upon request. This paper does not report original code. Any additional information required to reanalyze the data reported in this paper is available from the lead contact upon request.

EXPERIMENTAL MODEL AND SUBJECT DETAILS

Animals

The BKS.Cg-Dock7^{m}+/+Lepr^{db}/J (i.e., *db/db*) (Stock No: 000642) and the *Pten*$^{flox/flox}$ (Stock NO: 006440) mice were purchased from the Jackson Laboratory (Bar Harbor, ME, USA). The *Pax7*$^{CreERT2/CreERT2}$;*R26*$^{YFP/YFP}$ mice were described previously and generated in house (Zhou et al., 2021). All experiments were performed using 1-6-month-old mice. Except for the experiments in Figure S1D where only male mice were used, both male and female mice were used for other *in vivo* studies as no obvious gender-specific differences were noticed. All animal-based experiments were performed in accordance with protocols approved by the Animal ethics committee at HKUST.

Human skeletal muscle biopsies

Human skeletal muscles that remained attached to tendons were collected from nine patients (seven males and two females aged between 18-55 years old) who underwent the "anterior cruciate ligament reconstruction" surgery following the protocol approved by the Institutional Review Board at the Prince of Wales Hospital (Shatin, Hong Kong).

METHOD DETAILS

Isolation of MuSCs by fluorescence-activated cell sorting (FACS)

To obtain human MuSCs (hMuSCs), collect muscles that remained attached to tendon graft after the anterior cruciate ligament reconstruction (ACLR) surgery. 2∼2.4 g of human muscles was minced first with a scalpel and then scissors, and digested by 10 mL collagenase II (1000 U/mL) (#LS004177; Worthington Biochemical Corp) in Ham's F10 with 10% horse serum (washing medium) at 37°C for 90 min. To obtain mouse MuSCs, mice were sacrificed by cervical dislocation and hindlimb muscles were dissected, minced, and digested by collagenase II (800 U/mL) in Ham's F10 with 10% horse serum at 37°C for 90 min. Digested human or mouse muscles were triturated and washed once by washing medium. Then, muscles were subjected to another digestion with collagenase II (80 U/mL) and Dispase (1 U/mL) (#17105041, Thermo Fisher) for 30 min. The cell suspensions were passed through a syringe fitted with a 20 Gauge needle for 15 times followed by filtration through a 40 μm Nylon Cell Strainer (BD Biosciences). To isolate hMuSCs, single-cell suspensions were incubated with the following antibodies (all antibodies were used at a dilution of 1:75) for 45 min: CD31-Alexa Fluor 488, CD45-Alexa Fluor 488, CD34-FITC, ITGB1-APC and NCAM-Biotin, and then with a secondary antibody (Streptavidin-PE at a dilution of 1:125) for 15 min followed by FACS-mediated isolation of hMuSCs (NCAM$^+$ITGB1$^+$CD31$^-$/CD45$^-$/CD34$^-$). For mice carrying a YFP reporter, single-cell suspensions were directly loaded to a cell sorter for isolation of YFP$^+$ MuSCs. For mice without a YFP reporter, single-cell suspensions were incubated with the following antibodies (all antibodies were used at a dilution of 1:75) for 45 min: CD31-FITC, CD45-FITC, Sca1-Alex 647 and Vcam1-Biotin, and then a secondary antibody (Streptavidin-PE-Cy7) for 15 min followed by FACS-mediated isolation of MuSCs (CD31$^-$/CD45$^-$/Sca1$^-$/Vcam1$^+$). Based on Pax7 immunostaining, more than 90% of mouse or human MuSCs isolated by the FACS schemes above were Pax7$^+$ (see Figures S2A and S7).

Isolation of single myofibers

The extensor digitorum longus (EDL) muscles were carefully dissected and digested by collagenase II (800 U/mL) at 37°C for 75 min, followed by gentle trituration with a glass pipette in washing medium to release single myofibers. The intact myofibers were picked by a blue tip that was pre-coated with filtered horse serum.

Muscle injury by cardiotoxin (CTX) or $BaCl_2$ injection

Adult mice were anesthetized by intraperitoneal injection of Avertin (0.5 mg/g body weight). To injure TA muscles, we injected 30 μL of either CTX (10 μM) in 0.9% NaCl or $BaCl_2$ (1.2%) into TA muscles to induce acute muscle injury. For lower hindlimb muscle injury, a total of 50 μL of CTX (10 μM) was injected into 8 spots in lower hindlimb muscles. Muscles were then collected at various time points for histological, immunostaining or FACS analysis.

Hematoxylin and eosin (H&E) staining

TA muscles were dehydrated in 20% sucrose and embedded in O.C.T. Embedded muscles were sectioned to 8 μm slices using a Leica Cryostat. TA muscle sections were fixed with 4% paraformaldehyde (PFA) for 10 min and rinsed with water. Fixed muscle sections were immersed in hematoxylin staining solution for 30 min followed by differentiating in 1% HCl and neutralizing in ammonia solution, with water rinsing after each step. This was followed by eosin staining for 3 min and sequential dehydration in 70% ethanol, 80% ethanol, 95% ethanol, 100% ethanol, 50% ethanol with 50% xylene and 100% xylene before mounting.

Immunostaining

Cells or myofibers were fixed with 4% PFA for 5 min, washed with PBS with 0.1% Triton (0.1% PBST) for 3 times, permeabilized in 0.5% PBST for 20 min and subsequently blocked in 4% IgG-free BSA for at least 1 h at room temperature. After removal of the blocking solution and washing, samples were incubated with a primary antibody at 4°C overnight followed by washing and incubating with a secondary antibody and 100 ng/mL of 4′,6-diamidino-2-pheny-lindole (DAPI) for another 1 h. After washing with 0.1% PBST, slides were mounted with Mowiol and imaged by fluorescence microscopy. Immunostaining of muscle sections was performed similarly as described above, except that 0.3% PBST was used for washing. For Pax7 and eMHC staining on muscle sections, antigen retrieval was carried out by boiling sections in 0.01 M of citric acid (pH 6.0) at 90°C twice (5 min/each time) prior to blocking. For EdU labeling, cells or myofibers were cultured with 10 μM of EdU during labeling. After fixation, the click chemistry reaction was performed according to manufacturer's instructions.

Western blot

Cells were washed with PBS and lysed in lysis buffer (50 mM Tris, pH 7.4, 1% Triton, 150 mM NaCl, 10% glycerol, supplemented with protease and phosphatase inhibitors) for 10 min, followed by sonication. Samples were then centrifuged at 13,000 rpm for 10 min and soluble whole cell lysates were collected. 20∼50 μg of cell lysates was heat-denatured in SDS sample buffer and proteins were separated by 8%-12% SDS-PAGE followed by protein transfer to PVDF membrane. The membrane was first blocked with 10% milk in 0.1% TBST for 1 h, then incubated with a primary antibody overnight at 4°C or 3-4 h at room temperature, followed by incubation with a secondary antibody for 1 h at room temperature. After washing, the enhanced chemiluminescence (ECL) solution and the ChemiDoc Image System were used to detect signals.

EdU labelling

5-Ethynyl-2′-deoxyuridine (EdU) from the Click-iT EdU Alexa Fluor 488 Imaging Kit (Thermo Fisher) was used to label proliferating cells, The EdU was dissolved in DMSO and added to cells or myofibers at a final concentration of 10 μM. For *in vivo* EdU labeling, 1.5 days post-injury (dpi), EdU (5 μL of 10 mM solution/g) was injected into mice intraperitoneally every 6 h for 3 doses. Mice were sacrificed at 2.5 dpi and MuSCs were isolated by FACS and immediately subjected to EdU staining.

The AMP/ATP assay

The concentration of intracellular ATP and AMP was determined by the ATP/ADP/AMP Assay Kit (Biomedical Research Service & Clinical Application) following manufacturer's instructions. The bioluminescence of each sample was measured on a Lumat LB 9507 Ultra Sensitive Tube Luminometer (Berthold Technologies).

The Seahorse Cell Mito Stress assay

The oxygen consumption rate (OCR) was measured by a Seahorse XFp Analyzer (Agilent, CA, USA) using the "Cell Mito Stress" test kit. 5 x 10^4 of FISCs were seeded into each well of a miniplate and cultured in growth medium (F10 plus 10% horse serum). The day before the assay, a sensor cartridge was hydrated in Agilent Seahorse XF Calibrant at 37°C in a non-CO_2 incubator overnight. During the day of assays, the growth medium was substituted with XF DMEM (pH 7.4) supplemented with 1 mM of pyruvate, 2 mM of glutamine and 1 g/L of glucose and cells were incubated in a non-CO_2 incubator at 37°C for 1 h. The "Cell Mito Stress" assays were performed following manufacturer's instructions. The final concentration of different ETC inhibitors used in the assays were as follows: 2.5 μM of Oligomycin A, 5 μM of FCCP, 2 μM of Rotenone and 1.5 μM of Antimycin A.

RNA-seq and data processing

~8 x 10^5 of FISCs from each of the three mice were divided in three wells and cultured with or without 0.1 mM of Ado or 0.25 mM of AMP for 24 h. Total RNA was extracted with the NucleoSpin RNA XS kit (MACHEREY-NAGEL) following manufacturer's instructions. cDNA was then synthesized and amplified according to the Smart-Seq2 protocol (Picelli et al., 2014). Purified cDNA was then fragmented using Tn5 followed by library construction using the TruePrep® DNA Library Prep Kit V2 for Illumina (Vazyme, Nanjing, China). Over 25 million paired-end sequencing reads were obtained for each sample. Raw sequencing reads were mapped to the mouse reference genome (GRCm38/mm10) using STAR aligner. The raw counts table was generated with FeatureCount, followed by differential gene expression analysis with the DEseq2 R package. Differentially expressed genes with absolute log2 fold change >1 and padj <0.05 were considered significant. Raw data were uploaded to GEO (GEO: GSE175786). For GSEA, the DEseq2 normalized count table was used as an input file using default parameters. Two gene set databases, Hallmark and C5 (Gene ontology), were used for differential pathway enrichment. False discovery rate (FDR) *q* values were calculated by gene permutation and gene sets with FDR *q* value less than 5% were selected.

QUANTIFICATION AND STATISTICAL ANALYSIS

Image quantification

Cell sizes, cross-section areas of myofibers, and the fluorescence intensity of Tomm20 were quantified using Fiji (https://imagej.net/software/fiji/). The fluorescence intensity of pS6 was quantified by CellProfiler (https://cellprofiler.org/).

Statistical analysis

All error bars represent standard deviation (s.d.). The experimental data were analyzed with GraphPad Prism. Data were analyzed with unpaired, two-tailed Student's *t*-test when comparing two groups.